haematologica
Journal of the Ferrata Storti Foundation

Deep phenotyping of nodal T-cell lymphomas reveals immune alterations and therapeutic targets

by Pierre Stephan, Jimmy Perrot, Allison Voisin, Maud Barbery, Thibault Andrieu, Maxime Grimont, Julie Caramel, Mathilde Bardou, Garance Tondeur, Edoardo Missiaglia, Philippe Gaulard, François Lemonnier, Laurence de Leval, Emmanuel Bachy, Pierre Sujobert, Laurent Genestier, Alexandra Traverse-Glehen, and Yenkel Grinberg-Bleyer

Received: October 16, 2023.
Accepted: May 17, 2024.

Citation: Pierre Stephan, Jimmy Perrot, Allison Voisin, Maud Barbery, Thibault Andrieu, Maxime Grimont, Julie Caramel, Mathilde Bardou, Garance Tondeur, Edoardo Missiaglia, Philippe Gaulard, François Lemonnier, Laurence de Leval, Emmanuel Bachy, Pierre Sujobert, Laurent Genestier, Alexandra Traverse-Glehen, and Yenkel Grinberg-Bleyer.
Deep phenotyping of nodal T-cell lymphomas reveals immune alterations and therapeutic targets.
Haematologica. 2024 May 30. doi: 10.3324/haematol.2023.284448 [Epub ahead of print]

Deep phenotyping of nodal T-cell lymphomas reveals immune alterations and therapeutic targets

Pierre Stephan[1], Jimmy Perrot[2], Allison Voisin[1], Maud Barbery[1], Thibault Andrieu[1], Maxime Grimont[1], Julie Caramel[1], Mathilde Bardou[2], Garance Tondeur[2], Edoardo Missiaglia[3], Philippe Gaulard[4], François Lemmonier[4], Laurence de Leval[3], Emmanuel Bachy[2,5], Pierre Sujobert[2,5], Laurent Genestier[5], Alexandra Traverse-Glehen[2], Yenkel Grinberg-Bleyer[1]

Affiliations: [1] Cancer Research Center of Lyon, UMR INSERM 1052, CNRS 5286, Université Claude Bernard Lyon 1, Labex DEV2CAN, Centre Léon Bérard, Lyon, France.

[2] Centre Hospitalier Lyon Sud and Université Claude Bernard Lyon-1, Pierre- Bénite, France.

[3] Institute of Pathology, Department of Laboratory Medicine and Pathology, Lausanne University Hospital and Lausanne University, Lausanne, Switzerland.

[4] AP-HP, Henri Mondor Hospital, Pathology Department, Créteil, France; University Paris Est Créteil, INSERM, IMRB, Créteil, France.

[5] Centre International de Recherche en Infectiologie (CIRI), Team Lymphoma Immuno-Biology, UMR INSERM U1111, CNRS 5308, Université Claude Bernard Lyon I, ENS de Lyon, Lyon, France.

Author contributions: P. Stéphan, JP, AV, M. Barbery, TA, M. Bardou, and GT performed experiments and analyzed data. MP, MG, JC, EM, PG, LDL, EB, LG and YGB analyzed data. PG, FL, LDL, EB, P. Sujobert, LG and ATG selected patient samples and confirmed the original diagnosis through pathological analyses. YGB supervised the study, wrote the paper and secured funding.

Running head: *Immune microenvironment in nodal PTCLs*

Corresponding author: Yenkel Grinberg-Bleyer, yenkel.grinberg-bleyer@inserm.fr

Data-sharing statement: All raw or analyzed data will be made available upon reasonable request, by e-mail to the corresponding author.

Acknowledgements: We thank the CeVi_Collection group: (https://experts-recherche-lymphome.org/calym/explorer-les-ressources-du-consortium/collection-cevi/centres-participants-a-la-collection-cevi/) from the CALYM Carnot Institute funded by the French National Research Council (ANR), for providing cell suspension samples from PTCL patients. We thank the biological resource centers of Montpellier, Toulouse and Creteil for providing the fixed tissue samples obtained at diagnosis, used for re-assessment of the original diagnosis. We are grateful to Maud Plaschka (CCRI, Vienna, Austria) for bioinformatics analyses. We thank Pierre Milpied (CIML, Marseille, France), as well as all members of the lab, for helpful discussions on the project.

Funding: This project was funded by grants from la Ligue contre le Cancer, the ATIP-Avenir funds, and the Laboratory of excellence (LabEx) Dev2Can (ANR-10-LABX-0061), to YGB. PS was supported by a scholarship from the Fondation pour la Recherche Médicale (FRM). AV was supported by a fellowship from the Association pour la Recherche contre le Cancer (ARC) Foundation.

Authors' disclosures: EM reports research funding from Astra-Zeneca. PG reports consultancy for Gilead and Takeda; and research funding from Alderan, Innate Pharma, Sanofi, and Takeda. FL reports research funding from Institut Roche and travel grant from Gilead. LdL reports consultancy for AbbVie, Bayer, Bio Ascend, Lunaphore, Novartis. EB reports consultancy or lecture fees from Incyte, Roche, Takeda, ADCTherapeutics, Novartis, Kite/ GILEAD, Miltenyi, Janssen, Sanofi; travel expense reimbursement from Roche, Gilead, Abbvie; and research funding from Agmen, Bristol-Myers Squibb and Daiichi Sankyo. P. Sujobert reports consultancy or lecture fees from Gilead/Kyte, Janssen Cylag, BMS/Cellgene, Abbvie; and research funding from Astra-Zeneca and Servier. The other authors have no conflict of interest to disclose.

Abstract

Whereas immunotherapies have revolutionized the treatment of different solid and hematological cancers, their efficacy in nodal peripheral T-cell lymphomas (PTCLs) is limited, due to a lack of understanding of the immune response they trigger. To fully characterize the immune tumor microenvironment (TME) of PTCLs, we performed spectral flow cytometry analyses on 11 angioimmunoblastic T-cell lymphomas (AITL), 7 PTCL, not otherwise specified (PTCL, NOS) lymph node samples, and 10 non-tumoral control samples. The PTCL TME contained a larger proportion of regulatory T cells and exhausted CD8+ T cells, with enriched expression of druggable immune checkpoints. Interestingly, CD39 expression was up-regulated at the surface of most immune cells, and a multi-immunofluorescence analyses on a retrospective cohort of 43 AITL patients demonstrated a significant association between high CD39 expression by T cells and poor patient prognosis. Together, our study unravels the complex TME of nodal PTCLs, identifies targetable immune checkpoints, and highlights CD39 as a novel prognostic factor.

Introduction

PTCLs are highly heterogeneous neoplasms derived from post-thymic T cells or mature Natural Killer (NK) cells, and represent 10% to 15% of non-Hodgkin lymphomas [1]. The two most common subtypes in Western countries are angioimmunoblastic T-cell lymphomas (AITL) and peripheral T-cell lymphomas, not otherwise specified (PTCL, NOS). Malignant cells in AITL are predominantly $CD4^{+}CD8^{-}$ and characterized by the expression of T follicular helper cell (TFH) markers such as ICOS or PD-1 [2]. PTCL-NOS display heterogeneous phenotypes that do not match any other category and represent about 20% of PTCLs [3]. Despite advances in the understanding and classification of these neoplasms over the past decades their prognosis remains poor, with a 5-year overall survival (OS) around 30%, fostering the need to identify new therapeutic targets. Moreover, though immune checkpoint inhibitors that target inhibitory receptors, such as PD-1/PD-L1 blocking agents, have been successfully used in some

hematologic malignancies [4, 5] , their clinical benefits in nodal PTCL are relatively modest [6, 7], and several cases of hyperprogression have even been reported in patients with different PTCLs[6, 8] likely due to the expression of PD-1 by neoplastic cells [9].

Transposing checkpoint-blockade-based immunotherapies to nodal PTCLs, has been hindered by our poor understanding of the types and phenotypes of immune cells recruited in response to these tumors. Studies focusing on the contribution of the tumor microenvironment (TME) to PTCL progression, reported that monocytes as well as immunosuppressive $CD163^+$ macrophages were suggested to promote disease worsening [10, 11], whereas high levels of B cells and dendritic cells (DCs), and a high CD8/CD4 T-cell ratio were associated with better survival [12, 13], although these latter findings were recently challenged [14]. Though generally of poor prognosis in most cancers[15] , the proportion and prognostic value of immunosuppressive Foxp3+ regulatory T cells in PTCLs are still unclear [16, 17]. Finally, a recent study using Cytof and scRNA-seq approaches revealed the expression of exhaustion markers by tumor-infiltrating $CD8^+$ T cells, as well as perturbations in the B-cell compartment of patients with AITL [18]. In this study, we aimed to bridge this knowledge gap and extensively characterize the phenotype of immune cells recruited in response to PTCLs.

Methods

Samples for spectral flow cytometry analyses

Frozen lymph node (LN) cell suspensions from 18 PTCL samples, collected at diagnosis, were obtained through the CeVi_Collection Project from the CALYM Carnot Institute (Lyon, France). Samples were collected as part of a RIPH3 project (ID RCB 2020-A02273-36 validated by the CPP Ile de France V on November 26, 2020 n°20.07.28.49748). Reactive LN suspensions were obtained from the biological resource center of Lyon-Sud Hospital (agreement CRB BB-0033-00046). Tissues were assessed by the pathology department and cancer diagnosis was excluded through pathological evaluation and absence of T or B clonality. All adult patients (≥ 18) gave their informed written consent on the secondary use of their samples for research. The clinical and biological data of the patients were collected retrospectively. Their characteristics are presented in Tables S1 and S2.

Blood samples from healthy volunteers were obtained through the Etablissement Français du Sang (EFS). Peripheral blood mononuclear cells (PBMCs) were isolated by Ficoll density gradient centrifugation and red blood cells were lysed with Ammonium-Chloride-Potassium lysis Buffer. Tonsils obtained anonymously from five donors that underwent tonsillectomy were used as a control (Clinique du Parc, Lyon, agreement #1A16502305468). Tonsils were reduced to cell suspensions by mechanical disruption followed by enzymatic digestion with 2 mg/mL collagenase-D (Roche) and 20 U/mL DNase (Sigma). The resulting cell suspensions were filtered, washed and frozen.

Samples for multi-IF analyses

43 tissue blocks of formalin-fixed and paraffin-embedded (FFPE) AITL samples collected at diagnosis, were obtained from the department of Pathology at the Lyon-Sud Hospital. This study was performed according to the principles of the Declaration of Helsinki. Patients had provided an informed consent. The study was approved by the local ethics committee (MR-004 #23-5211). Clinical and biological data of the patients were collected retrospectively. Summary of the data is presented in Tables S3 and S4.

Flow cytometry

1 million live cells were stained through successive incubation steps with dyes and antibodies (Abs). The complete list of Abs and their final concentration can be found in Table S5. Acquisition was performed on an Aurora Spectral Cytometer (Cytek). Analyses were done using the OMIQ software (Dotmatics) (www.omiq.ai). Details on the experimental protocol and analyses can be found in the supplemental methods section; the number of cells analyzed in each subset is detailed in Tables S6 and S7.

Tissue micro-arrays, multi-IF protocol and data analysis

Representative tumor areas were selected on H&E slides by an experienced pathologist. 4-plex mIF assay (CD3, CD8, CD39 and DAPI) was performed using a modified 7-color TSA protocol template. Slides were imaged using the Vectra Polaris spectral imaging system (Perkin Elmer). Scans were visualized with the Phenochart software. Cell segmentation and phenotypes were

identified via InForm version 2.4.8 (Akoya Biosciences). Parameters were analyzed using R version 4.2.1. Detailed information can be found in the supplemental methods.

Statistical analyses

Statistics were performed using GraphPad Prism Software v9 and R version 4.2.1. For FACS data, Kruskall-Wallis or 2-way ANOVA tests were used, unless mentioned otherwise. Statistical analyses for comparison between clusters established by the FlowSOM algorithm, were done using the edgeR package. PFS was calculated from the date of diagnosis to the date of progression, relapse, or death from any cause. OS was calculated from the date of diagnosis to the date of death from any cause. Survival estimates were calculated with the Kaplan-Meier method. Survival distributions were compared with the log-rank test, and Cox proportional hazard regression models were used to estimate hazard ratios and associated 95% confidence intervals.

Results

PTCL-specific immune cell populations identified through deep immunophenotyping

To document immune phenotypes associated with PTCLs, we designed a 33-color flow cytometry panel to identify different innate and adaptive subsets in a single tube, namely DCs, macrophages, NK and B cells, and a number of markers to distinguish subsets of T cells. Moreover, activation, proliferation and exhaustion of these populations were determined using different intracellular and surface markers (Table 1 and Table S5). We applied this immunophenotyping panel to lymph node (LN) cell suspensions obtained from 18 nodal PTCL patients at diagnosis (11 AITL and 7 PTCL, NOS, Tables S1 and S2), as well as 5 non-tumoral reactive LN, 5 tonsil samples and 5 PBMC samples obtained from healthy donors. Of note, progression-free survival (PFS) and overall survival (OS) of our PTCL cohort corroborated previous reports (Figure S1A).

To identify disease-specific cell populations, we first normalized the data to attenuate the batch effect, concatenated all lymphoid tissue (tumoral LN, non-tumoral tonsil, reactive LN) samples and carried out a series of unsupervised analyses. PBMCs were not included in these analyses

to avoid major changes in cell-type distribution (data not shown). Two-dimensional reduction through Uniform Manifold Approximation and Projection (UMAP) and computer-driven clustering through FlowSOM conducted on cell type markers (CD3, CD4, CD8, CD56, TCRγδ, CD163, CD11c, CD20), identified 18 clusters, largely corresponding to classical immune lineages (T cells, NK cells, B cells, DCs) (Figure 1A, B and Tables S6 and S7). Interestingly, this unsupervised analysis revealed a clear distinction between samples from PTCL patients and non-tumoral samples (Figure 1A, Figure S1B). Specifically, we detected tissue-specific B-cell and T-cell clusters, and noted that DCs (cluster #14) were higher in both AITL and PTCL-NOS samples compared to control LN or tonsil samples (Figure 1B). Two patient-specific clusters with aberrant phenotypes, namely clusters #13 ($CD3^+CD4^-CD8^-$) and #7 ($CD3^+CD4^+CD20^+$) were differentially represented between NOS and AITL samples, though the proportion of the remaining cell subtypes were very close. Supervised analyses based on traditional manual gating revealed strong decrease in B cells in PTCL samples compared to non-tumoral tissues, and an increase in DCs (Figure 1C, Figure S2). $CD4^+$ and $CD8^+$ T cells were also more abundant in PTCLs compared to tonsil samples but not reactive LN. Of note, NK cells ($CD7^+CD56^+$) were slightly more abundant without reaching statistical significance.

To assess the putative link between the abundance of cell types and their proliferation, we measured Ki67 expression, and found a systematic increase in proliferating $CD4^+$ and $CD8^+$ T cells in malignant samples (Figure 1D). A trend toward B-cell proliferation was observed in PTCL, NOS samples compared to controls. This was not the case in AITL samples, likely because TFH features of tumor cells enhance B-cell activation, maturation and proliferation [19].

Analysis of CD4+ T-cell subsets in PTCLs

Next, we analyzed the features of $CD4^+Foxp3^-$ conventional (Tconv) cells, that contained both transformed and normal cells, in PTCL compared to tonsils and reactive LN. Based on histological evaluation at diagnosis, all patients of our AITL cohort displayed a $CD3^+CD4^+CD8^-Foxp3^-$ tumor cell phenotype, whereas two of our PTCL-NOS patients, harbored a $CD3^+CD4^-CD8^-$ phenotype (Figure 1B and Table S2). We used UMAP and FlowSOM algorithms with T-cell

markers, proliferation/activation proteins and checkpoint receptors as variables (Figure 2A). Cells were highly activated in all samples, with only a minority of $CD45RA^+$ naïve-like cells (Figure 2B). We identified 21 clusters, corresponding to cells expressing divergent levels of CD7/CD10, Ki67 and many checkpoints, including TFH markers, such as ICOS and PD-1. Strikingly, a series of clusters from PTCL samples were clearly separated from control samples on the UMAP, highlighting that transformation deeply impacted the Tconv cell phenotype either in an intrinsic or extrinsic manner (Figure 2C). Indeed, control samples harbored significantly more classical $CD7^+PD\text{-}1^+ICOS^+CXCR5^+$ TFH cells than PTCL (Clusters #5,19,20), whereas AITL samples comprised discrete and specific phenotypes, including $CD10^+$ and/or $CD7^-$ cells as expected, but also showing high expression of LAG-3 (cluster #15), or OX-40 (cluster #8). In PTCL, NOS, we observed patient-specific clusters, such as a cytotoxic phenotype (patient 11, cluster 11) and a $TCR\gamma\delta^+$ malignancy (patient 20, cluster 2). Tconv cells from AITL patients were also highly heterogeneous, with variable expression of checkpoints (Figure S3A, B). Because of this heterogeneity, hierarchical clustering failed to fully discriminate reactive LN from PTCL samples (Figure S3C). Analysis through manual gating confirmed strong expression of PD-1 and ICOS in AITL (>50% cells expressing ICOS, PD-1 or both), but without reaching statistical significance. Interestingly, the proportion of PD1+ICOS+ double positive cells in PTCL, NOS samples was reduced compared to tonsils and AITL, showing that most cells did not adopt a full TFH-like phenotype (Figure 2D). Thus, in addition to TFH markers widely used for diagnosis, we show that CD4+ T cells from AITL samples adopt a highly activated state, often characterized by heterogeneous expression of different checkpoint molecules.

Given that tumoral PTCL T cells can lose the expression of surface CD3 (sCD3), we also looked for aberrant cell phenotypes in the sCD3-negative compartment. Among the 23 clusters identified within these cells, we found B cells, NK cells or DCs, as expected (Figure S4A, B). Interestingly, several other cell populations were more abundant in PTCL samples (Figure S4C). These included cluster #5, retrieved in 2 patients, that matched a $CD4^+$ $checkpoint^+$ TFH-like phenotype, similar to that found in $sCD3^+$ Tconv cells, and that were likely to be malignant. The cytotoxic phenotype of patient 11 was also found within a sCD3-negative cluster (#03). In addition to this,

we found 2 aberrant $CD4^{-}Foxp3^{+}CD39^{+}$ clusters (#09 and 15) only found in patient 9 and 25 but which did not match the phenotype of their $sCD3^{+}$ counterpart (Figure 2B, D).

To further harness the complexity of these tumor cell phenotypes, we next analyzed each sample individually in order to ascertain that no rare cell cluster was overlooked. We specifically looked for clusters of cells presenting a non-classical phenotype, i.e., T cells harboring loss of CD7, gain of CD10 or aberrant expression of surface or intracellular proteins. This strategy led to the identification of putative neoplastic phenotypes in most but not all samples (Table S8). Interestingly, in 3 PTCL, NOS samples, cell clusters exhibiting co-expression of PD-1 and ICOS could be found; thus, a diagnosis of nodal follicular helper T-cell lymphoma, NOS could not be fully excluded in these cases. In line with our previous observations, we detected a very high heterogeneity between samples. Importantly, in about half of the cases, we found more than one aberrant phenotype, indicating that PTCLs, as shown in many other cancers, are also prone to intra-tumor heterogeneity.

The data thus illustrate both the complexity of proper tumor-cell identification in nodal PTCL, and the perturbations of immune homeostasis in these diseases. This also warrants the use of additional tools (TRBC1 staining, TCR clonality at the single-cell level) to better understand the biology of nodal PTCL.

$Foxp3^{+}$ Treg cells are critical inhibitors of anti-tumor immunity. We detected a significant increase in the proportion of Treg cells among $CD4^{+}$ T cells in both AITL and PTCL-NOS compared to tonsil and LN samples (Figure S5A). Based on classical activation markers and Treg cell hallmarks, 6 cell clusters were identified through FlowSOM, corresponding to $CD45RA^{+}$ naïve (cluster #6), $PD1^{+}ICOS^{+}$ TFR-like (#4), $CD39^{bright}TIGIT^{hi}$ (#1) cells, as well as a subset with high expression of multiple Treg markers (#2) (Figure S5B-C). Cluster #5 was specific to patient PTCL-NOS #11. Of those populations, we only found a decrease in naïve-like $TCF1^{+}CD45RA^{+}$ cells in AITL compared to tonsils but not LNs; this was confirmed through supervised analysis (Figure S5D). Collectively, Treg cells were abundant in PTCLs and exhibited a high activation profile, suggesting active immunosuppression.

NK cell phenotype is not impaired in PTCLs

NK cells are important effectors of the anti-tumor response; nevertheless, their activation and function are often dampened in cancer, constituting an important mechanism of immune escape. We analyzed the distribution and activation/maturation levels of $CD56^+$ NK cells. Unsupervised analyses revealed 6 clusters that could be generally defined as $CD56^{bright}$ cytokine-producing cells, $CD57^+$ cytotoxic cells and $Ki67^+$ proliferating cells (Figure S6A-B). These different populations were not significantly different between control and PTCL samples, with the exception of a slight increase in total $GZMB^+$ cells in AITL, detected through supervised analysis and manual gating (Figure S6B-E). Thus, the PTCL TME did not seem to significantly impact NK cell distribution.

$CD8^+$ T cells display features of exhaustion

Next, we examined the phenotype of $CD8^+$ T cells in lymphoid tissues. FlowSOM analysis on 17 markers of activation highlighted 18 distinct cell clusters that corresponded to (i) $CD45RA^+$ $TCF1^{+/-}$ naïve-like cells, with low expression of checkpoint molecules (ii) $Ki67^+$ proliferating cells, (iii) $GZMB^+$ cells devoid of checkpoint expression, and (iv) $CD45RA^-$ activated/memory cells with the expression of at least 2 checkpoint receptors (Figure 3A-B). There were clear differences between tissues (Figure 3C). Differential expression analyses between subgroups of samples, highlighted the loss of naïve-like cells ($CD45RA^+TCF1^+GZMB^-$) in both AITL and PTCL-NOS (clusters #12, 16, 17) compared to non-malignant tissues (Figure 3 B, D). In contrast, $Ki67^+$ cells increased (Figure 1D), and clusters # 1, 4, 6 and 7, corresponding to cell subsets with very strong co-expression of PD-1 and TIM-3 among other inhibitory receptors, were significantly enriched in tumor samples. Although variable, the total number of $PD\text{-}1^+TIM\text{-}3^+$ cells was higher in tumor cells compared to tonsils and reactive LN (Figure 3E). Unsupervised clustering efficiently distinguished PTCLs from tonsils, but not reactive LN samples, based exclusively on the phenotype of $CD8^+$ T cells (Figure S7). Of note, $CD8^+$ T cell profiles were not strikingly different between AITL and PTCL-NOS patients, revealing common features of T-cell immunity between the two lymphoma subtypes. We further investigated the phenotype of these cells by performing Boolean analysis following manual gating, and observed a strong increase in cells expressing at

least 3 inhibitory receptors in tumor samples compared to healthy tonsils and LN (Figure 3F). This exhausted phenotype, together with the expansion of Treg cells, suggest that a strong immune suppression takes place in PTCL lymph nodes, emphasizing the need for immunotherapeutic strategies in these conditions.

Differential expression of actionable receptors on immune cell subsets

We thus wondered whether our strategy may unveil actionable costimulatory molecules, *i.e.,* surface checkpoints with specific expression patterns in pro-tumoral subsets (Treg cells and Tconv cells containing tumor cells) versus anti-tumoral populations ($CD8^+$ and NK cells). We first analyzed inhibitory checkpoints. As previously described [18], PD-1 was broadly expressed (average of 40-60% positive cells) across subsets (NK cells being negative for this receptor, as shown in other contexts [20]) (Figure 4), similarly to TIM-3 (9-57%) and TIGIT (30-70%). Conversely, LAG-3 was expressed by few cells and CTLA-4 was mostly found on Treg and Tconv cells (18-84% positive cells), while its expression was quite low on $CD8^+$ T cells and NK cells; this was particularly true for AITL samples. In addition, NKG2A was expressed by about 50% of NK cells regardless of the pathology, and undetected on T cells. Concerning 'activation' checkpoints, ICOS and OX-40 followed a pattern similar to CTLA-4, whereas 4-1BB and TNFR2 displayed low expression, the latter being preferentially expressed by Treg cells. Thus, while checkpoint receptors were generally broadly expressed in PTCLs, some of these targetable proteins (CTLA-4, ICOS, OX-40) showed specific expression patterns with high expression in Tconv (including tumor cells) and Treg cells and low expression in anti-tumor effectors, indicating that they may be considered as therapeutic targets.

Increased CD39 expression in PTCL is associated with poor prognosis

In addition to these checkpoints, belonging to the CD28 and tumor necrosis factor receptor superfamilies, we also investigated the expression levels of the ectonucleotidase CD39. CD39 is a surface protein that has recently emerged as an important immune checkpoint in cancer, through its ability to convert ATP to AMP, ultimately leading to the production of the immunosuppressive nucleoside adenosine [21]. While CD39 was mostly expressed by DC, B cells and NK cells in tonsils and non-tumoral LN, it was expressed by some T cells in PTCL patients

(Figure 5A-B). In $CD8^+$ T cells, CD39 was largely enriched in activated cells compared to naïve cells, and to a higher extent, in exhausted T cells (Figure S8A). To investigate whether this tumor-specific CD39 expression by T cells was associated with other immune perturbations, we split our 18-sample cohort into CD39 low, intermediate and high groups (Figure S8B). No correlation with major immune subtypes could be found (Figure S8C). Interestingly, increase in CD39 expression was associated with enhanced TIM-3/PD-1 and CTLA-4-positive $CD8^+$ T cells subsets, although this did not reach significance (Figure S8D). Conversely, high CD39 expression was correlated with lower GZMB expression, likely indicative of immune dysfunction sustaining tumor progression. We thus wondered whether CD39 expression impacted PTCL clinical outcome. First, we investigated the putative prognostic value of CD39 at the RNA level, in bulk samples, by examining the association between *ENTPD1* expression and OS in the TENOMIC cohort, that consists of a dataset of microarray-defined gene expression profiles of 85 LN samples of AITL patients. In this cohort, the level of *ENTPD1* expression in total cells was not significantly associated with a prognostic value (Figure S8E). To further explore the expression of CD39 at the protein level in T-cell subsets, we used a multi-immunofluorescence (IF) approach, on tissue microarrays (TMA) comprising 43 LN samples from AITL patients at diagnosis, with a 10-year clinical history (Tables S3 and S4). PFS and OS in the cohort matched previously reported data (Figure S8F). Slides were stained for CD3, CD8, CD39 and DAPI and the proportion of each population was determined. $CD3^+$ T cells, in particular the $CD8^+$ subset, exhibited higher CD39 expression compared to non-T cells. As in FACS analyses, we observed an important variability in CD39 expression between patients (Figure 5C, D). We first measured the impact of CD39 expression in different subsets by splitting the samples based on the median expression of CD39. Although the proportion of $CD39^+$ cells among total cells was not associated with prognostic significance, patients harboring high CD39 expression among T cells (regardless of CD8 expression) showed a trend toward poorer prognosis (Figure S8G). To refine this analysis, we analyzed the data following Receiver Operating Characteristic (ROC) curve-based separation of patients. We found that patients harboring the highest expression of CD39 in T cells (n = 15, 35% of the whole cohort) exhibited a significantly poorer prognosis, both at the PFS and OS levels (Figure 5E). Similar conclusions were reached when analyzing CD39 expression in the

$CD3^+CD8^+$ and $CD3^+CD8^-$ subsets (Figure S8H). The prognostic value of CD39 expression by T cells, was further confirmed through multivariate Cox models including Prognostic Index for AITL (PIAI), sex and age (Figure 5F). Together, our data that suggest CD39 expression by T cells may represent a novel independent prognostic factor in AITL and should be explored as a putative target.

Discussion

To date, and at odds with many solid tumors and other hematological malignancies, there is a clear lack of knowledge in the distribution and phenotype of immune cells in the context of PTCLs. Our study documents an accumulation of highly activated and heterogeneous T-cell populations -whereas B-cell were less abundant in this disease. Although this confirms recently reported data [18], this does not preclude the therapeutic targeting of B cells, as these can support tumor cells [22, 23].

One striking observation that can be made based on our data is the large phenotypic heterogeneity of Tconv cells between PTCL patients. Although most Tconv cells expressed at least one checkpoint surface receptor, only about half of them expressed PD-1 or ICOS, suggesting that the phenotype and biology of AITL cells extend beyond these 2 single markers. This deserves further exploration, for instance by combining high-dimensional cytometry to single-cell TCR-Seq that allows the identification of clonal cell populations. Most $CD8^+$ T cells in both AITL and PTCL, NOS expressed at least one inhibitory checkpoint and a prominent $PD\text{-}1^+TIM3^+$ population could be detected, suggesting that an active exhaustion process might be taking place in PTCL tissues. This is in accordance with observations made in patients with cutaneous T-cell lymphoma and other non-Hodgkin lymphomas [24-26], and confirms the potential benefit of checkpoint-based immunotherapies in PTCLs.

In this regard, we aimed at identifying surface receptors expressed by cytotoxic T cells and/or NK cells but not by Tconv cells (that included most malignant cells) and Treg cells, or vice-versa. Similar to the large spectrum of PD-1 expression that may explain the hyperprogression detected

in some PTCL patients following PD-1 blockade, we observed that TIGIT and TIM-3 were largely expressed by both tumor-promoting (tumor cells, Treg cells) and tumor-inhibiting ($CD8^+$ T cells, NK cells) populations. This broad expression may negate the therapeutic potential of blocking Abs that are currently under clinical development in solid and hematologic malignancies [27]. In contrast, other surface markers, such as OX-40, or to a lesser extent CTLA-4 or ICOS, displayed a much higher expression on $CD4^+$ (comprising tumor cells and Treg cells) than other subsets. These may thus represent attractive therapeutic targets for the treatment of PTCLs. In line with this, mRNA expression of *CTLA4* was shown to be associated with poor prognosis in a meta-analysis of PTCL transcriptomes[28]. Specifically, this would require the use of depleting monoclonal Abs (mAbs) through the use of Ab-dependent cellular cytotoxicity and phagocytosis - optimized IgG1 molecules [29]. To date and to our knowledge, OX-40 mAbs that are under development have agonistic functions and should not be recommended for the treatment of PTCLs. The depleting effect of current anti-CTLA-4 mAbs, such as Ipilimumab, is still largely debated and there is room for improvement [30, 31]. Different strategies have been used to create anti-CTLA4 IgG1 mAbs with strong Treg-depleting properties and anti-tumor effects in preclinical models [32, 33], which deserve attention for the therapy of PTCLs. MEDI-570, an afucosylated IgG1 anti-ICOS mAb, was shown to induce T-cell depletion in cynomolgus monkeys[34]; a phase I trial reported positive signs of activity in AITL patients [35]. In addition to these T-cell-targeting agents, NKG2A also appears to be an interesting target in PTCLs, as its expression was largely restricted to NK cells. As blocking anti-NKG2A mAbs are currently in clinical evaluation in solid cancers [36], they may represent a future therapeutic avenue in PTCLs.

In addition to these traditional immune checkpoints, our data highlights CD39 as a promising target in nodal PTCLs, both through its prognostic value and its potential therapeutic targeting. The combined action of CD39 and CD73 that lead to the production of adenosine, have been extensively described for their tumor-promoting functions in solid cancers [21]. CD39 inhibition reinvigorates cytotoxic T-cell activity in preclinical models of melanoma or sarcoma among others [37]. CD39 expression also increases in different hematologic malignancies, including T-cell-derived cancers such as Adult T-cell leukemia/lymphoma or Sezary syndrome [38, 39]. High expression of CD39 was shown to be associated with poor prognosis in Diffuse Large B-Cell

Lymphoma and multiple myeloma [40, 41]. CD39 expression on T cells is correlated with disease severity in patients with chronic lymphocytic leukemia [42, 43]. Because of this association with tumor progression, the therapeutic potential of CD39 inhibition has largely been tested in blood cancers. For instance, mAbs targeting CD39 potentiate the therapeutic efficacy of T-cell transfer in a humanized model of B-cell lymphoma [44], whereas ARL67156 and POM-1, two ectonucleotisase inhibitors with high affinity for CD39, enhance T-cell function in follicular lymphoma and multiple myeloma patient samples; respectively [41, 45]. CD73 or A2AR inhibition enhance non-tumoral T-cell proliferation in Sezary syndrome *in vitro* [46]. Our data now extend the tumor-promoting properties of CD39 to nodal PTCLs. We propose that CD39 expression could be assessed by immunohistochemistry and/or flow cytometry as a potent prognostic factor in AITL. Moreover, patients with PTCL may benefit from the CD39-blocking agents currently under clinical development for other cancers.

References

1. Campo E, Jaffe ES, Cook JR, et al. The International Consensus Classification of Mature Lymphoid Neoplasms: a report from the Clinical Advisory Committee. Blood. 2022;140(11):1229-1253.
2. Fujisawa M, Chiba S, Sakata-Yanagimoto M. Recent Progress in the Understanding of Angioimmunoblastic T-cell Lymphoma. J Clin Exp Hematop. 2017;57(3):109-119.
3. de Leval L, Parrens M, Le Bras F, et al. Angioimmunoblastic T-cell lymphoma is the most common T-cell lymphoma in two distinct French information data sets. Haematologica. 2015;100(9):e361-364.
4. Armand P, Shipp MA, Ribrag V, et al. Programmed Death-1 Blockade With Pembrolizumab in Patients With Classical Hodgkin Lymphoma After Brentuximab Vedotin Failure. J Clin Oncol. 2016;34(31):3733-3739.
5. Ansell SM, Lesokhin AM, Borrello I, et al. PD-1 blockade with nivolumab in relapsed or refractory Hodgkin's lymphoma. N Engl J Med. 2015;372(4):311-319.
6. Bennani NN, Kim HJ, Pederson LD, et al. Nivolumab in patients with relapsed or refractory peripheral T-cell lymphoma: modest activity and cases of hyperprogression. J Immunother Cancer. 2022;10(6):e004984.
7. Shi Y, Wu J, Wang Z, et al. Efficacy and safety of geptanolimab (GB226) for relapsed or refractory peripheral T cell lymphoma: an open-label phase 2 study (Gxplore-002). J Hematol Oncol. 2021;14(1):12.
8. Ratner L, Waldmann TA, Janakiram M, Brammer JE. Rapid Progression of Adult T-Cell Leukemia-Lymphoma after PD-1 Inhibitor Therapy. N Engl J Med. 2018;378(20):1947-1948.
9. Wartewig T, Kurgyis Z, Keppler S, et al. PD-1 is a haploinsufficient suppressor of T cell lymphomagenesis. Nature. 2017;552(7683):121-125.
10. Wilcox RA, Wada DA, Ziesmer SC, et al. Monocytes promote tumor cell survival in T-cell lymphoproliferative disorders and are impaired in their ability to differentiate into mature dendritic cells. Blood. 2009;114(14):2936-2944.
11. Ham JS, Park HY, Ryu KJ, Ko YH, Kim WS, Kim SJ. Elevated serum interleukin-10 level and M2 macrophage infiltration are associated with poor survival in angioimmunoblastic T-cell lymphoma. Oncotarget. 2017;8(44):76231-76240.
12. Sugio T, Miyawaki K, Kato K, et al. Microenvironmental immune cell signatures dictate clinical outcomes for PTCL-NOS. Blood Adv. 2018;2(17):2242-2252.

13. Zhu Q, Deng X, Yao W, et al. Novel tumour-infiltrating lymphocyte-related risk stratification based by flow cytometry for patients with de novo angioimmunoblastic T cell lymphoma. Ann Hematol. 2021;100(3):715-723.
14. Chen Z, Zhu Q, Deng X, et al. Angioimmunoblastic T-cell lymphoma with predominant CD8+ tumor-infiltrating T-cells is a distinct immune pattern with an immunosuppressive microenvironment. Front Immunol. 2022;13:987227.
15. Ohue Y, Nishikawa H. Regulatory T (Treg) cells in cancer: Can Treg cells be a new therapeutic target? Cancer Sci. 2019;110(7):2080-2089.
16. Lundberg J, Berglund D, Molin D, Kinch A. Intratumoral expression of FoxP3-positive regulatory T-cells in T-cell lymphoma: no correlation with survival. Ups J Med Sci. 2019;124(2):105-110.
17. Bruneau J, Canioni D, Renand A, et al. Regulatory T-cell depletion in angioimmunoblastic T-cell lymphoma. Am J Pathol. 2010;177(2):570-574.
18. Pritchett JC, Yang ZZ, Kim HJ, et al. High-dimensional and single-cell transcriptome analysis of the tumor microenvironment in angioimmunoblastic T cell lymphoma (AITL). Leukemia. 2022;36(1):165-176.
19. Gaulard P, de Leval L. Follicular helper T cells: implications in neoplastic hematopathology. Semin Diagn Pathol. 2011;28(3):202-213.
20. Judge SJ, Dunai C, Aguilar EG, et al. Minimal PD-1 expression in mouse and human NK cells under diverse conditions. J Clin Invest. 2020;130(6):3051-3068.
21. Moesta AK, Li XY, Smyth MJ. Targeting CD39 in cancer. Nat Rev Immunol. 2020;20(12):739-755.
22. Fujisawa M, Nguyen TB, Abe Y, et al. Clonal germinal center B cells function as a niche for T-cell lymphoma. Blood. 2022;140(18):1937-1950.
23. Delfau-Larue MH, de Leval L, Joly B, et al. Targeting intratumoral B cells with rituximab in addition to CHOP in angioimmunoblastic T-cell lymphoma. A clinicobiological study of the GELA. Haematologica. 2012;97(10):1594-1602.
24. Querfeld C, Leung S, Myskowski PL, et al. Primary T Cells from Cutaneous T-cell Lymphoma Skin Explants Display an Exhausted Immune Checkpoint Profile. Cancer Immunol Res. 2018;6(8):900-909.
25. Heming M, Haessner S, Wolbert J, et al. Intratumor heterogeneity and T cell exhaustion in primary CNS lymphoma. Genome Med. 2022;14(1):109.
26. Yang ZZ, Liang AB, Ansell SM. T-cell-mediated antitumor immunity in B-cell non-Hodgkin lymphoma: activation, suppression and exhaustion. Leuk Lymphoma. 2015;56(9):2498-2504.
27. Ansell SM, Lin Y. Immunotherapy of lymphomas. J Clin Invest. 2020;130(4):1576-1585.
28. Li X, Liu Z, Mi M, et al. Identification of hub genes and key pathways associated with angioimmunoblastic T-cell lymphoma using weighted gene co-expression network analysis. Cancer Manag Res. 2019;11:5209-5220.
29. Yu J, Song Y, Tian W. How to select IgG subclasses in developing anti-tumor therapeutic antibodies. J Hematol Oncol. 2020;13(1):45.
30. Sharma A, Subudhi SK, Blando J, et al. Anti-CTLA-4 Immunotherapy Does Not Deplete FOXP3(+) Regulatory T Cells (Tregs) in Human Cancers-Response. Clin Cancer Res. 2019;25(11):3469-3470.
31. Quezada SA, Peggs KS. Lost in Translation: Deciphering the Mechanism of Action of Anti-human CTLA-4. Clin Cancer Res. 2019;25(4):1130-1132.
32. Ha D, Tanaka A, Kibayashi T, et al. Differential control of human Treg and effector T cells in tumor immunity by Fc-engineered anti-CTLA-4 antibody. Proc Natl Acad Sci U S A. 2019;116(2):609-618.
33. Semmrich M, Marchand JB, Fend L, et al. Vectorized Treg-depleting alphaCTLA-4 elicits antigen cross-presentation and CD8(+) T cell immunity to reject 'cold' tumors. J Immunother Cancer. 2022;10(1):e003488.
34. Nicholson SM, Carlesso G, Cheng LI, et al. Effects of ICOS+ T cell depletion via afucosylated monoclonal antibody MEDI-570 on pregnant cynomolgus monkeys and the developing offspring. Reprod Toxicol. 2017;74:116-133.
35. Chavez JC, Foss FM, MD, William BM, et al. A Phase I Study of Anti-ICOS Antibody MEDI-570 for Relapsed/Refractory (R/R) Peripheral T-Cell Lymphoma (PTCL) and Angioimmunoblastic T-Cell Lymphoma (AITL) (NCI-9930). Blood. 2020;136(supplement 1):5-6.
36. van Hall T, Andre P, Horowitz A, et al. Monalizumab: inhibiting the novel immune checkpoint NKG2A. J Immunother Cancer. 2019;7(1):263.

37. Perrot I, Michaud HA, Giraudon-Paoli M, et al. Blocking Antibodies Targeting the CD39/CD73 Immunosuppressive Pathway Unleash Immune Responses in Combination Cancer Therapies. Cell Rep. 2019;27(8):2411-2425.e9.
38. Nagate Y, Ezoe S, Fujita J, et al. Ectonucleotidase CD39 is highly expressed on ATLL cells and is responsible for their immunosuppressive function. Leukemia. 2021;35(1):107-118.
39. Bensussan A, Janela B, Thonnart N, et al. Identification of CD39 as a Marker for the Circulating Malignant T-Cell Clone of Sezary Syndrome Patients. J Invest Dermatol. 2019;139(3):725-728.
40. Nakamura K, Casey M, Oey H, et al. Targeting an adenosine-mediated "don't eat me signal" augments anti-lymphoma immunity by anti-CD20 monoclonal antibody. Leukemia. 2020;34(10):2708-2721.
41. Yang R, Elsaadi S, Misund K, et al. Conversion of ATP to adenosine by CD39 and CD73 in multiple myeloma can be successfully targeted together with adenosine receptor A2A blockade. J Immunother Cancer. 2020;8(1):e000610.
42. Perry C, Hazan-Halevy I, Kay S, et al. Increased CD39 expression on CD4(+) T lymphocytes has clinical and prognostic significance in chronic lymphocytic leukemia. Ann Hematol. 2012;91(8):1271-1279.
43. Aroua N, Boet E, Ghisi M, et al. Extracellular ATP and CD39 Activate cAMP-Mediated Mitochondrial Stress Response to Promote Cytarabine Resistance in Acute Myeloid Leukemia. Cancer Discov. 2020;10(10):1544-1565.
44. Li XY, Moesta AK, Xiao C, et al. Targeting CD39 in Cancer Reveals an Extracellular ATP- and Inflammasome-Driven Tumor Immunity. Cancer Discov. 2019;9(12):1754-1773.
45. Hilchey SP, Kobie JJ, Cochran MR, et al. Human follicular lymphoma CD39+-infiltrating T cells contribute to adenosine-mediated T cell hyporesponsiveness. J Immunol. 2009;183(10):6157-6166.
46. Sonigo G, Bozonnat A, Dumont M, et al. Involvement of the CD39/CD73/adenosine pathway in T-cell proliferation and NK cell-mediated antibody-dependent cell cytotoxicity in Sezary syndrome. Blood. 2022;139(17):2712-2716.

Cell populations	General phenotype	Activation checkpoints	Inhibitory checkpoints
Live/Dead	CD10	ICOS	PD-1
CD3 CD4 CD7	CXCR5 BCL6 Ki67	OX-40 4-1BB TNFR2	CTLA-4 TIM-3 LAG-3
CD8	EOMES	DNAM-1	NKG2A
FOXP3 CD56	T-BET GZMB		CD39 TIGIT
CD57 CD20	TCF-1 CD45RA		
CD11c			
CD163			
TCR$\gamma\delta$			

Table 1. Spectral flow cytometry panel

Figure legends

Figure 1. Perturbations in immune cell subsets in nodal peripheral T-cell lymphoma (PTCL) tissues. Samples were stained for FACS and analyzed using unsupervised clustering (A-C) and traditional supervised analyses (D, E) after manual gating on total live cells (see Figure S2). (A) Uniform Manifold Approximation and Projection (UMAP) visualization, FlowSOM distribution of clusters and projection of selected markers in concatenated samples after random selection of an equal number of cells between each group (5 tonsils, 5 reactive lymph nodes (LN), 11 angioimmunoblastic T-cell lymphomas (AITL), 7 PTCL, not otherwise specified (PTCL, NOS)). (B) Heatmap showing hierarchical clustering and expression (normalized across markers) of indicated markers in FlowSOM clusters, and their differential enrichment between groups. (C) Proportion of immune subsets using a supervised gating strategy. (D) Proportion of proliferating $Ki67^+$ cells across cell populations. Mean +/- SEM is shown, each dot represents a sample. Kruskal-Wallis tests were used. * $p < 0.05$, ** $p < 0.005$, *** $p < 0.001$, ns: non-significant.

Figure 2. Diverse phenotypes of $CD4^+$ Tconv cells in PTCL (A-D) Unsupervised clustering analyses following manual gating on live $CD3^+CD4^+Foxp3^-$ conventional T cells (Tconv). (A) UMAP visualization, FlowSOM distribution of clusters and projection of selected markers in concatenated samples after random selection of an equal number of cells between each group. (B) Heatmap showing hierarchical clustering and expression (normalized across markers) of indicated markers in FlowSOM clusters, and their differential enrichment between groups. (C) Distribution of cells from each group on UMAP. (D) Proportion of PD-1 and ICOS-expressing Tconv cells upon manual gating. Mean +/- SEM is shown. 2-way ANOVA tests were used; only the comparison of PD-1+ICOS+ cells between groups is shown. *p<0.05, ***p<0.001

Figure 3. PTCL-associated $CD8^+$ T cells adopt a highly activated, exhausted-like phenotype. (A) UMAP visualization, FlowSOM distribution of clusters and projection of selected markers in concatenated samples , following manual gating on live $CD8^+$ T cells and random selection of an equal number of cells between each group. (B) Heatmap showing hierarchical clustering and expression (normalized across markers) of indicated markers in FlowSOM clusters, and their differential enrichment between groups. (C) Distribution of cells from each

group on UMAP. (D-F) Proportion of naïve (D) and exhausted (D) $CD8^+$ T cells, and Boolean analysis of inhibitory checkpoint-expressing cells (F) upon manual gating. Mean +/- SEM is shown; each dot represents a sample. Kruskal-Wallis (D, E) and two-way ANOVA (F) tests were used. * $p < 0.05$, ** $p < 0.005$, *** $p < 0.001$.

Figure 4. Differential expression pattern of checkpoint receptors on immune subsets in PTCL. Proportion of checkpoint-expressing cells in different cell subsets following manual gating is shown as mean +/-SEM. Two-way ANOVA tests were used. * $p < 0.05$, ** $p < 0.005$, *** $p < 0.001$. Non-significant values are not displayed.

Figure 5. CD39 expression and prognostic value in PTCL. (A) UMAP visualization of CD39 expression across samples. (B) Proportion of $CD39^+$ cells across subsets and samples following manual gating. (C) Representative multi-immunofluorescence (multi-IF) staining in a $CD39^{high}$ (top) and a $CD39^{low}$ (bottom) sample. (D) Multi-IF quantification of $CD39^+$ cells across subsets and samples. (E) Kaplan-Meier curves of progression-free survival (PFS) and overall survival (OS). $CD39^{high}$ and $CD39^{low}$ samples were split upon Receiver operating characteristic (ROC) curve analyses (F) Hazard Ratio (HR, dots) and 95% confidence interval values (CI, bars) of the different parameters used in multivariate analyses. Two-way ANOVA (B, D), log-rank (E) and multivariate Cox regression (F) tests were used. * $p < 0.05$, ** $p < 0.005$, **** $p < 0.0001$

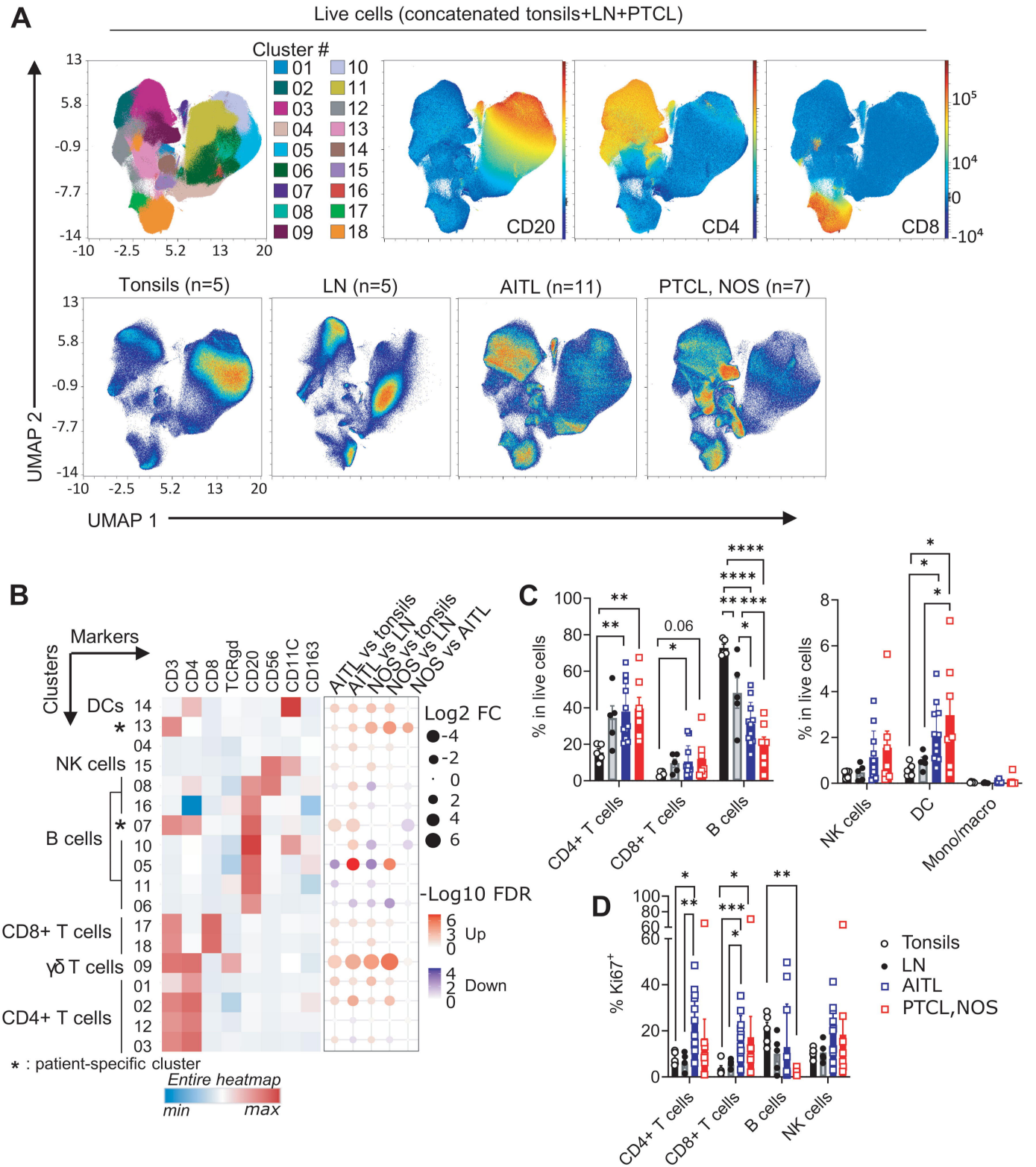
A
Live cells (concatenated tonsils+LN+PTCL)
Cluster #
01
02
03
04
05
06
07
08
09
10
11
12
13
14
15
16
17
18
CD20
CD4
CD8
Tonsils (n=5)
LN (n=5)
AITL (n=11)
PTCL, NOS (n=7)
UMAP 2
UMAP 1
B
Markers
Clusters
CD3
CD4
CD8
TCRgd
CD20
CD56
CD11C
CD163
AITL vs tonsils
AITL vs LN
NOS vs tonsils
NOS vs LN
NOS vs AITL
DCs
NK cells
B cells
CD8+ T cells
γδ T cells
CD4+ T cells
* : patient-specific cluster
Entire heatmap
min
max
Log2 FC
-Log10 FDR
Up
Down
C
% in live cells
CD4+ T cells
CD8+ T cells
B cells
NK cells
DC
Mono/macro
0.06
D
% Ki67+
Tonsils
LN
AITL
PTCL,NOS

Figure 1

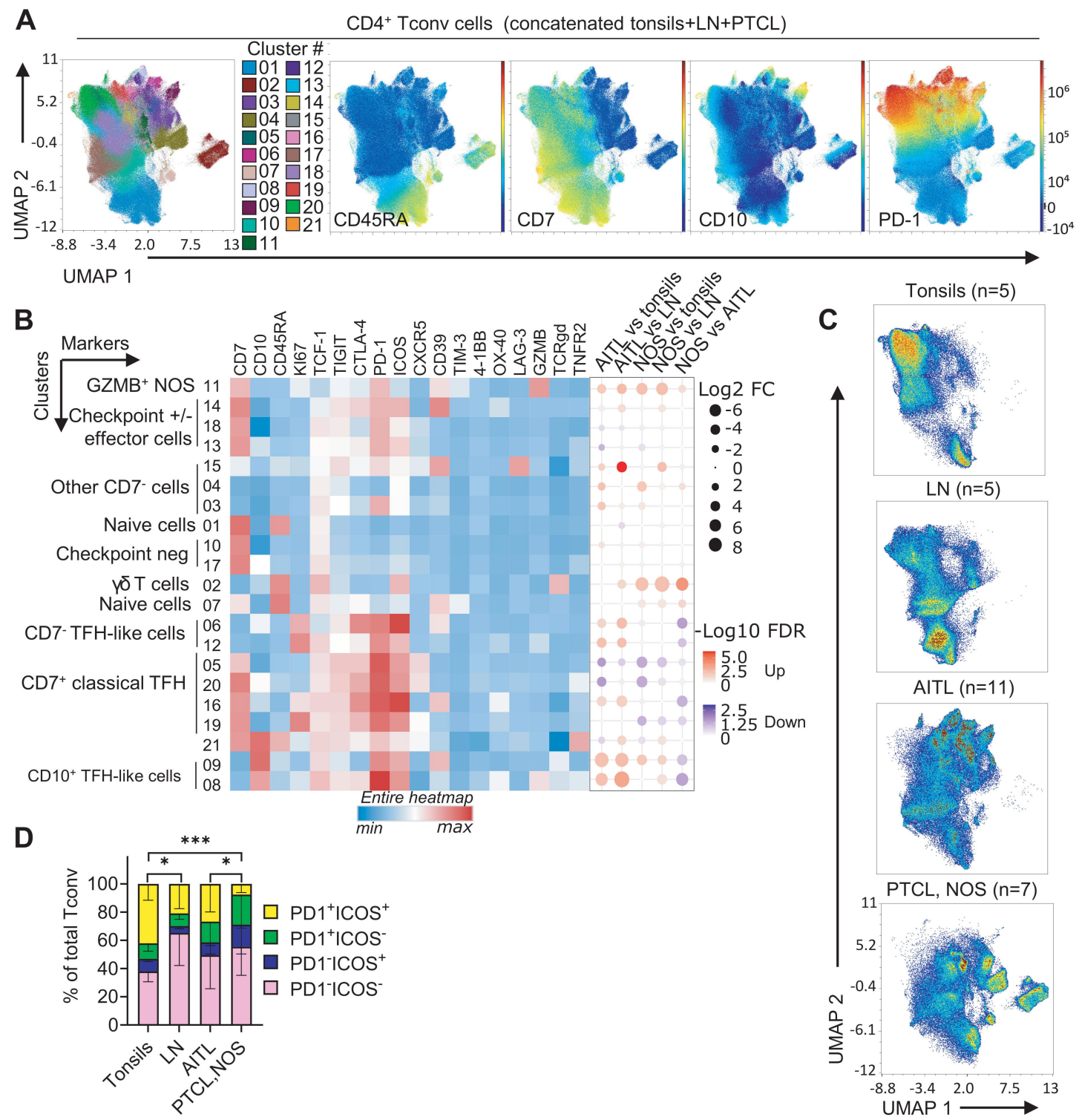
A
CD4+ Tconv cells (concatenated tonsils+LN+PTCL)
Cluster #
UMAP 2
UMAP 1
CD45RA
CD7
CD10
PD-1
B
Markers
Clusters
CD7 CD10 CD45RA KI67 TCF-1 TIGIT CTLA-4 PD-1 ICOS CXCR5 CD39 TIM-3 4-1BB OX-40 LAG-3 GZMB TCRgd TNFR2
AITL vs tonsils
AITL vs LN
NOS vs tonsils
NOS vs LN
NOS vs AITL
GZMB+ NOS
Checkpoint +/- effector cells
Other CD7- cells
Naive cells
Checkpoint neg
γδ T cells
Naive cells
CD7- TFH-like cells
CD7+ classical TFH
CD10+ TFH-like cells
Log2 FC
-Log10 FDR
Up
Down
Entire heatmap
min
max
C
Tonsils (n=5)
LN (n=5)
AITL (n=11)
PTCL, NOS (n=7)
UMAP 2
UMAP 1
D
% of total Tconv
PD1+ICOS+
PD1+ICOS-
PD1-ICOS+
PD1-ICOS-
Tonsils
LN
AITL
PTCL,NOS

Figure 2

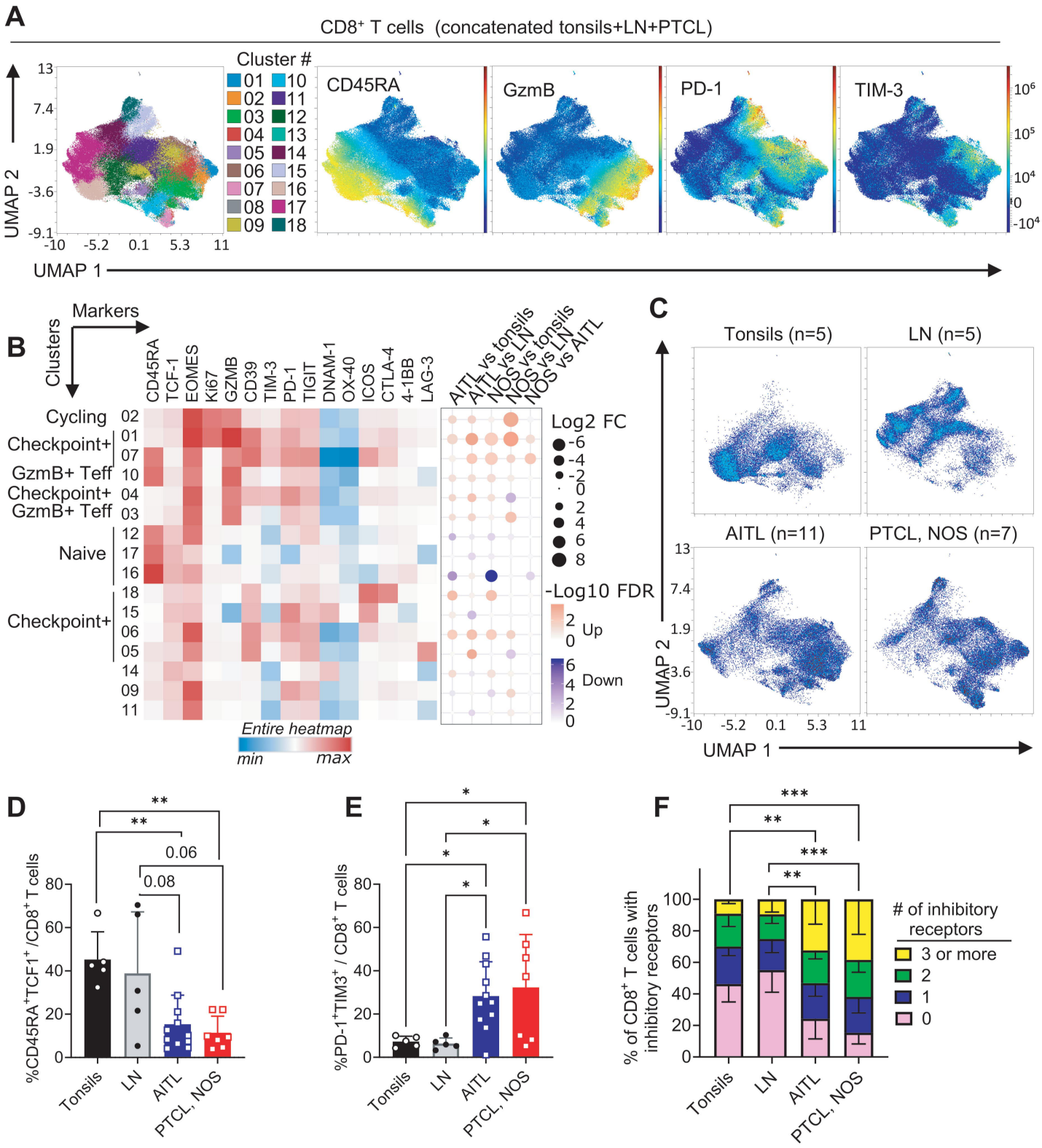
A
CD8+ T cells (concatenated tonsils+LN+PTCL)
Cluster #
CD45RA
GzmB
PD-1
TIM-3
UMAP 2
UMAP 1
B
Markers
Clusters
CD45RA
TCF-1
EOMES
Ki67
GZMB
CD39
TIM-3
PD-1
TIGIT
DNAM-1
OX-40
ICOS
CTLA-4
4-1BB
LAG-3
AITL vs tonsils
AITL vs LN
NOS vs tonsils
NOS vs LN
NOS vs AITL
Cycling
Checkpoint+
GzmB+ Teff
Checkpoint+ GzmB+ Teff
Naive
Checkpoint+
Log2 FC
-Log10 FDR
Up
Down
Entire heatmap
min
max
C
Tonsils (n=5)
LN (n=5)
AITL (n=11)
PTCL, NOS (n=7)
UMAP 2
UMAP 1
D
%CD45RA+TCF1+ /CD8+ T cells
0.06
0.08
Tonsils
LN
AITL
PTCL, NOS
E
%PD-1+TIM3+ / CD8+ T cells
F
% of CD8+ T cells with inhibitory receptors
# of inhibitory receptors
3 or more
2
1
0

Figure 3

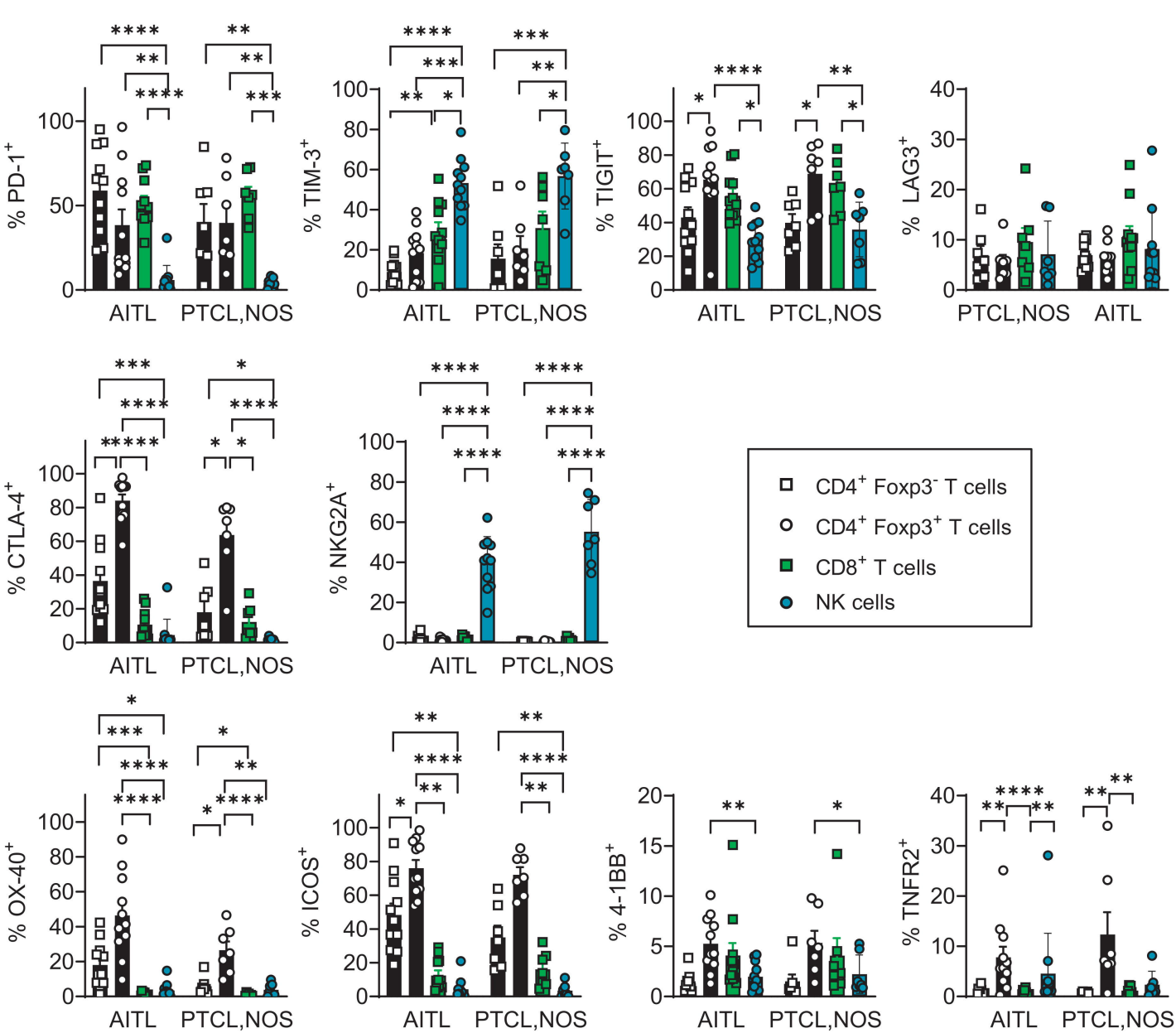
% PD-1+
% TIM-3+
% TIGIT+
% LAG3+
% CTLA-4+
% NKG2A+
% OX-40+
% ICOS+
% 4-1BB+
% TNFR2+
AITL
PTCL,NOS
CD4+ Foxp3- T cells
CD4+ Foxp3+ T cells
CD8+ T cells
NK cells

Figure 4

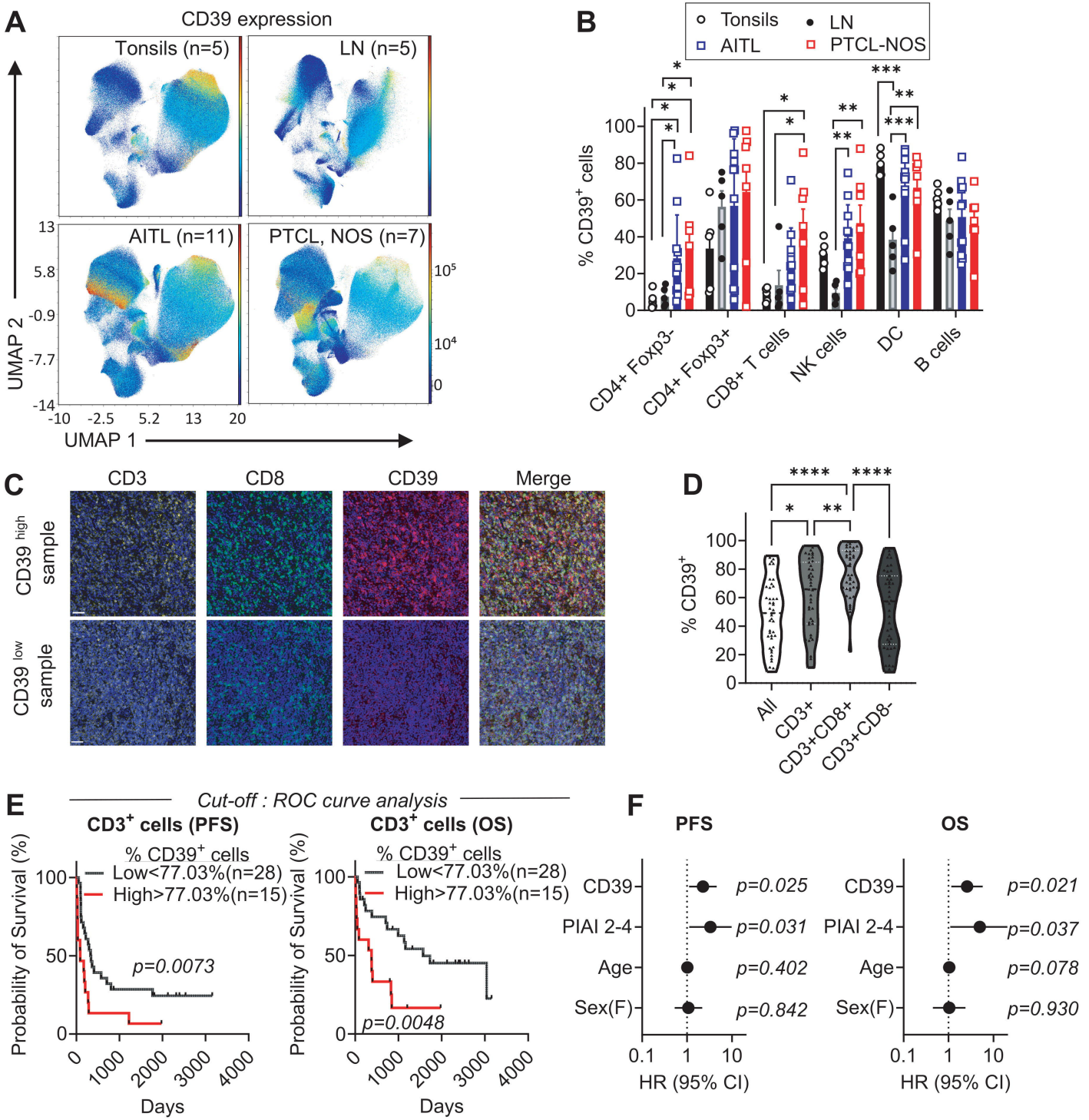
A
CD39 expression
Tonsils (n=5)
LN (n=5)
AITL (n=11)
PTCL, NOS (n=7)
UMAP 2
UMAP 1
B
Tonsils
LN
AITL
PTCL-NOS
% CD39+ cells
CD4+ Foxp3-
CD4+ Foxp3+
CD8+ T cells
NK cells
DC
B cells
C
CD3
CD8
CD39
Merge
CD39 high sample
CD39 low sample
D
% CD39+
All
CD3+
CD3+CD8+
CD3+CD8-
E
Cut-off : ROC curve analysis
CD3+ cells (PFS)
CD3+ cells (OS)
% CD39+ cells
Low<77.03%(n=28)
High>77.03%(n=15)
p=0.0073
p=0.0048
Probability of Survival (%)
Days
F
PFS
OS
CD39
PIAI 2-4
Age
Sex(F)
p=0.025
p=0.031
p=0.402
p=0.842
p=0.021
p=0.037
p=0.078
p=0.930
HR (95% CI)

Figure 5

Stephan et al., "Deep phenotyping of nodal T-cell lymphomas reveals immune alterations and therapeutic targets"

Supplementary material

- 8 supplementary Figures
- Supplementary figure legends
- 8 supplementary tables
- Supplementary methods

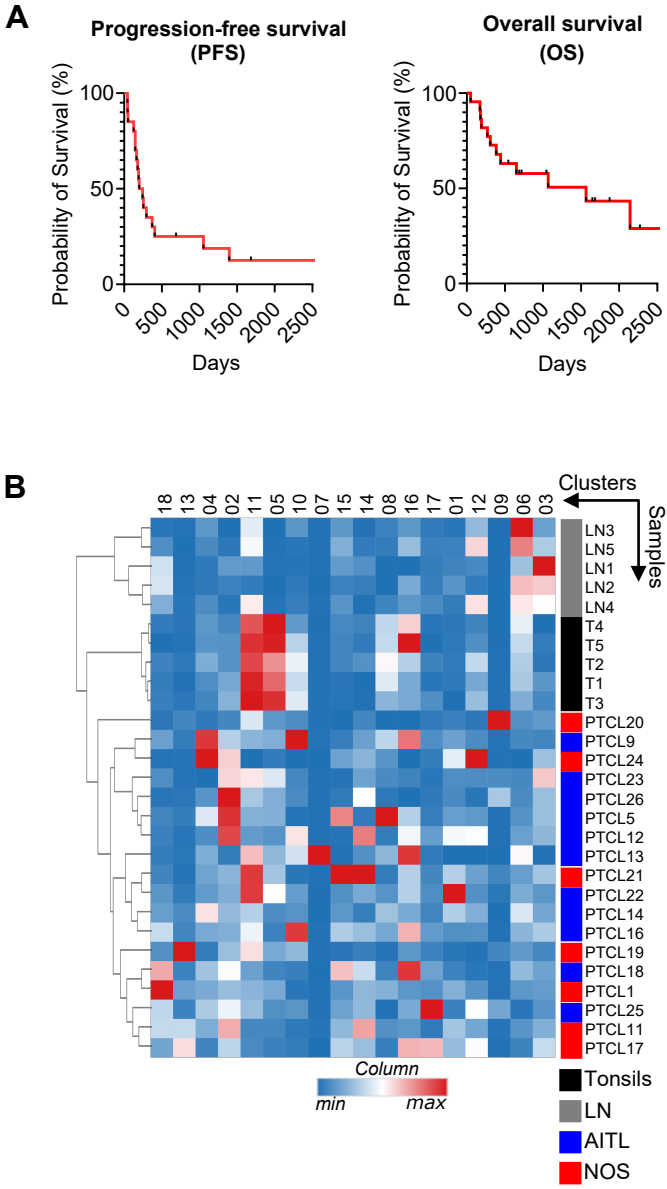
A
Progression-free survival
(PFS)
Probability of Survival (%)
100
50
0
0
500
1000
1500
2000
2500
Days
Overall survival
(OS)
Probability of Survival (%)
100
50
0
0
500
1000
1500
2000
2500
Days
B
Clusters
Samples
18
13
04
02
11
05
10
07
15
14
08
16
17
01
12
09
06
03
LN3
LN5
LN1
LN2
LN4
T4
T5
T2
T1
T3
PTCL20
PTCL9
PTCL24
PTCL23
PTCL26
PTCL5
PTCL12
PTCL13
PTCL21
PTCL22
PTCL14
PTCL16
PTCL19
PTCL18
PTCL1
PTCL25
PTCL11
PTCL17
Column
min
max
Tonsils
LN
AITL
NOS

Figure S1

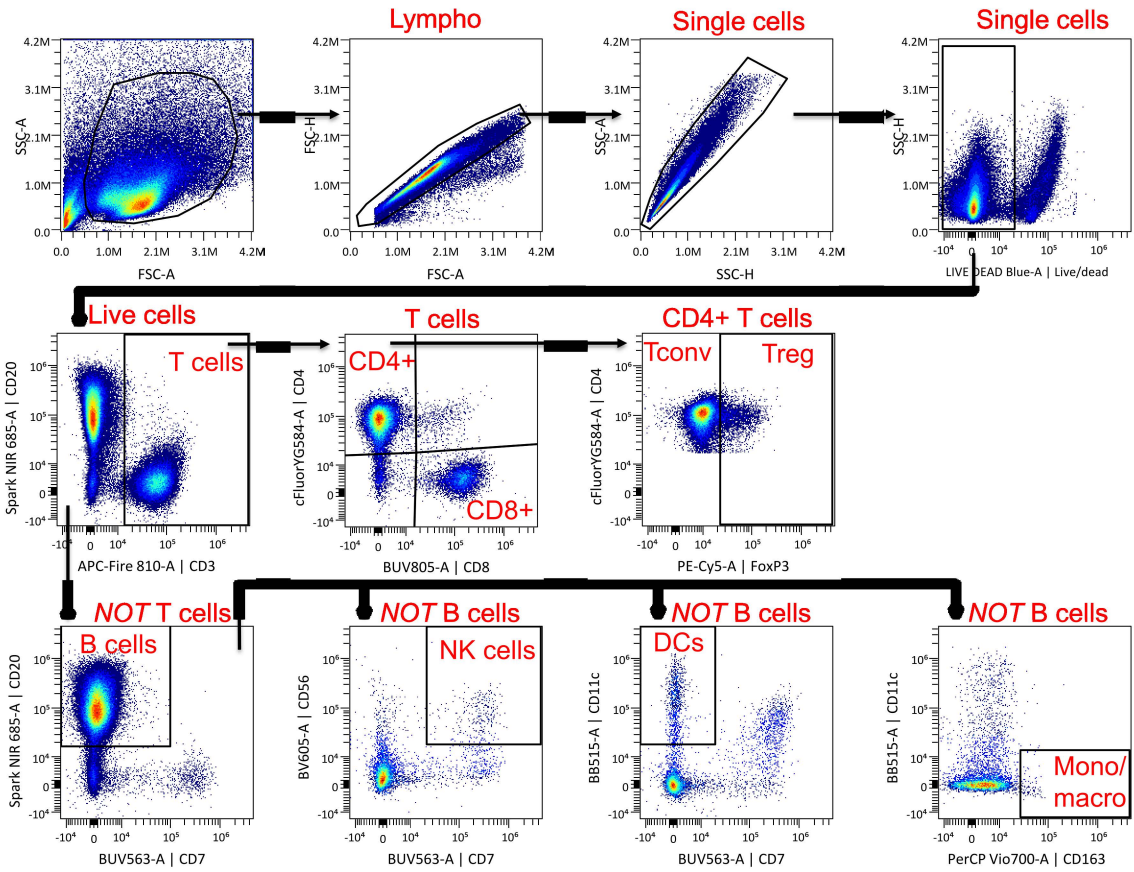
Lympho
Single cells
Single cells
SSC-A
FSC-A
FSC-H
FSC-A
SSC-A
SSC-H
SSC-H
LIVE DEAD Blue-A | Live/dead
Live cells
T cells
T cells
CD4+
CD8+
CD4+ T cells
Tconv
Treg
Spark NIR 685-A | CD20
APC-Fire 810-A | CD3
cFluorYG584-A | CD4
BUV805-A | CD8
cFluorYG584-A | CD4
PE-Cy5-A | FoxP3
NOT T cells
B cells
NOT B cells
NK cells
NOT B cells
DCs
NOT B cells
Mono/
macro
Spark NIR 685-A | CD20
BUV563-A | CD7
BV605-A | CD56
BUV563-A | CD7
BB515-A | CD11c
BUV563-A | CD7
BB515-A | CD11c
PerCP Vio700-A | CD163

Figure S2

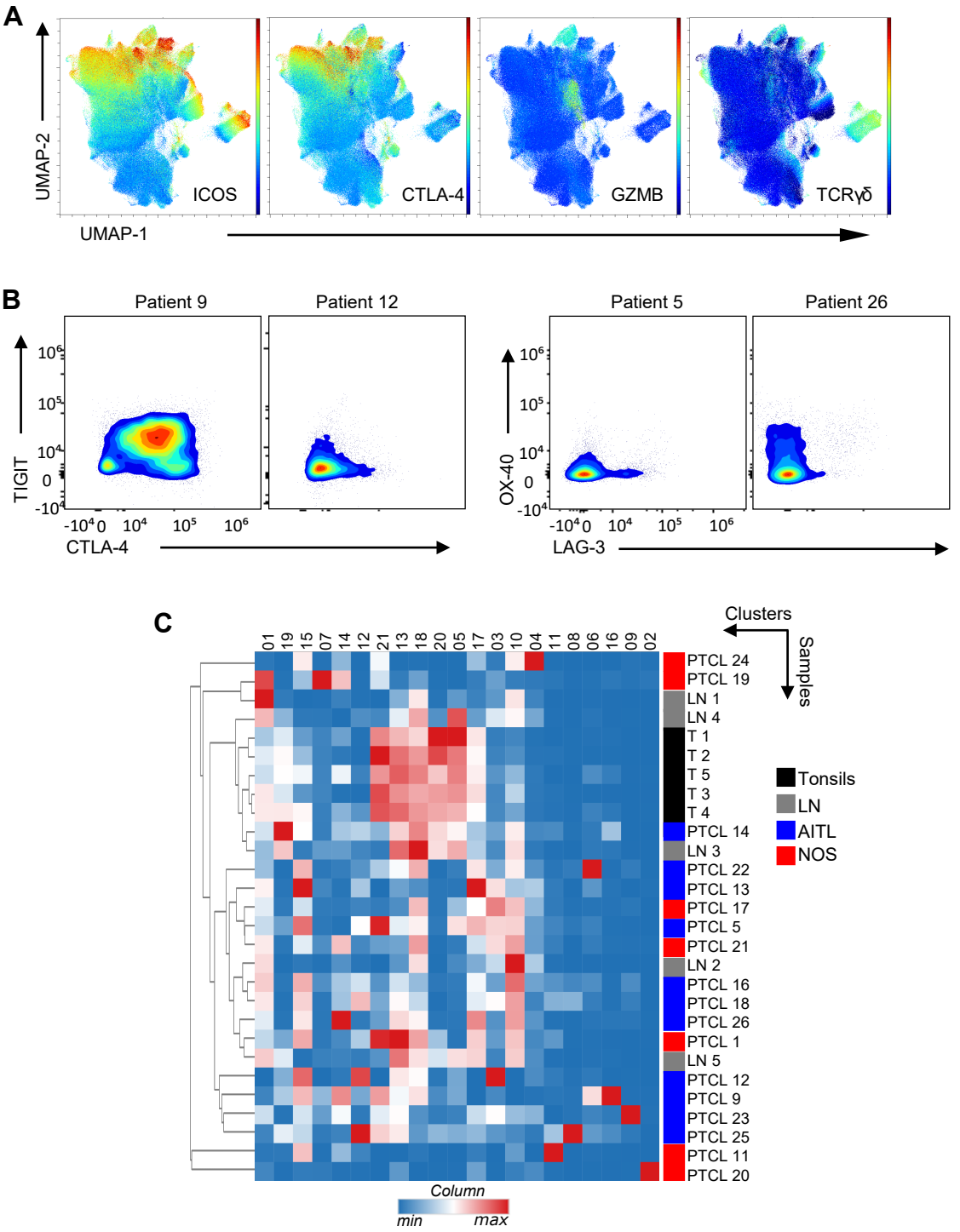
A
UMAP-2
UMAP-1
ICOS
CTLA-4
GZMB
TCRγδ
B
Patient 9
Patient 12
Patient 5
Patient 26
TIGIT
CTLA-4
OX-40
LAG-3
C
Clusters
Samples
PTCL 24
PTCL 19
LN 1
LN 4
T 1
T 2
T 5
T 3
T 4
PTCL 14
LN 3
PTCL 22
PTCL 13
PTCL 17
PTCL 5
PTCL 21
LN 2
PTCL 16
PTCL 18
PTCL 26
PTCL 1
LN 5
PTCL 12
PTCL 9
PTCL 23
PTCL 25
PTCL 11
PTCL 20
Tonsils
LN
AITL
NOS
Column
min
max

Figure S3

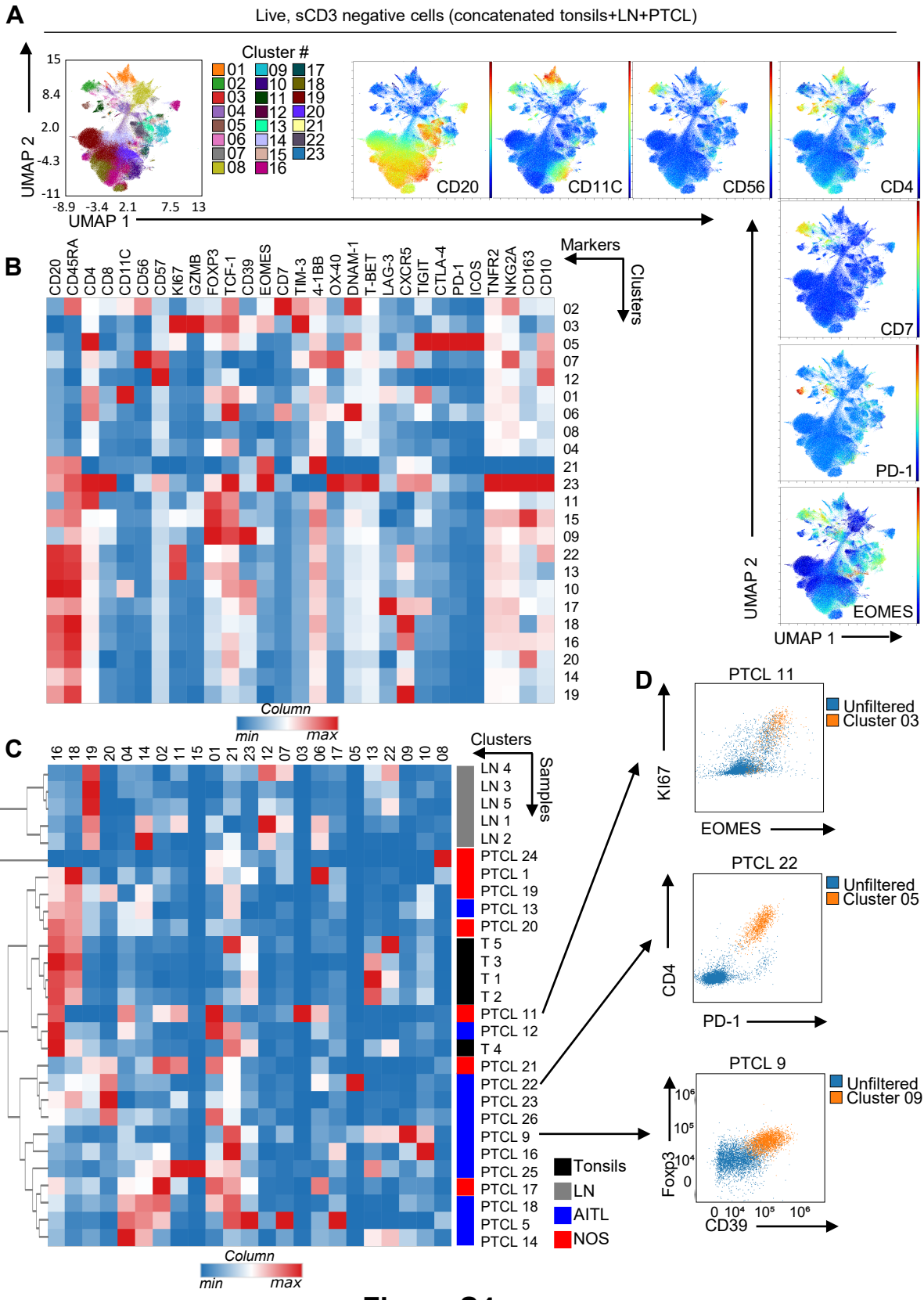
A
Live, sCD3 negative cells (concatenated tonsils+LN+PTCL)
Cluster #
UMAP 2
UMAP 1
CD20
CD11C
CD56
CD4
CD7
PD-1
EOMES
B
Markers
Clusters
CD20 CD45RA CD4 CD8 CD11C CD56 CD57 KI67 GZMB FOXP3 TCF-1 CD39 EOMES CD7 TIM-3 4-1BB OX-40 DNAM-1 T-BET LAG-3 CXCR5 TIGIT CTLA-4 PD-1 ICOS TNFR2 NKG2A CD163 CD10
02 03 05 07 12 01 06 08 04 21 23 11 15 09 22 13 10 17 18 16 20 14 19
Column
min
max
C
Clusters
Samples
16 18 19 20 04 14 02 11 15 01 21 23 12 07 03 06 17 05 13 22 09 10 08
LN 4 LN 3 LN 5 LN 1 LN 2 PTCL 24 PTCL 1 PTCL 19 PTCL 13 PTCL 20 T 5 T 3 T 1 T 2 PTCL 11 PTCL 12 T 4 PTCL 21 PTCL 22 PTCL 23 PTCL 26 PTCL 9 PTCL 16 PTCL 25 PTCL 17 PTCL 18 PTCL 5 PTCL 14
Tonsils
LN
AITL
NOS
Column
min
max
D
PTCL 11
KI67
EOMES
Unfiltered
Cluster 03
PTCL 22
CD4
PD-1
Unfiltered
Cluster 05
PTCL 9
Foxp3
CD39
Unfiltered
Cluster 09

Figure S4

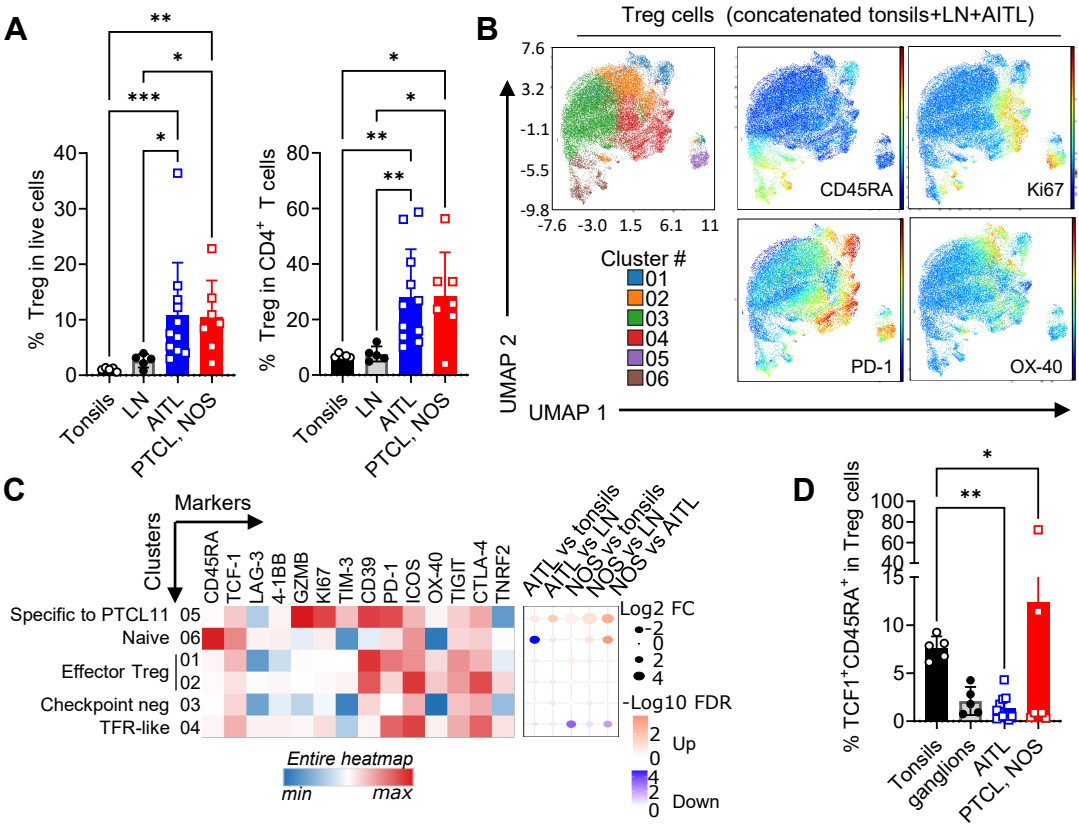
A
% Treg in live cells
% Treg in CD4+ T cells
Tonsils
LN
AITL
PTCL, NOS
B
Treg cells (concatenated tonsils+LN+AITL)
UMAP 1
UMAP 2
Cluster #
01
02
03
04
05
06
CD45RA
Ki67
PD-1
OX-40
C
Markers
Clusters
CD45RA
TCF-1
LAG-3
4-1BB
GZMB
KI67
TIM-3
CD39
PD-1
ICOS
OX-40
TIGIT
CTLA-4
TNRF2
Specific to PTCL11 05
Naive 06
Effector Treg 01
02
Checkpoint neg 03
TFR-like 04
AITL vs tonsils
AITL vs LN
NOS vs tonsils
NOS vs LN
NOS vs AITL
Log2 FC
-Log10 FDR
Up
Down
Entire heatmap
min
max
D
% TCF1+CD45RA+ in Treg cells
Tonsils
ganglions
AITL
PTCL, NOS

Figure S5

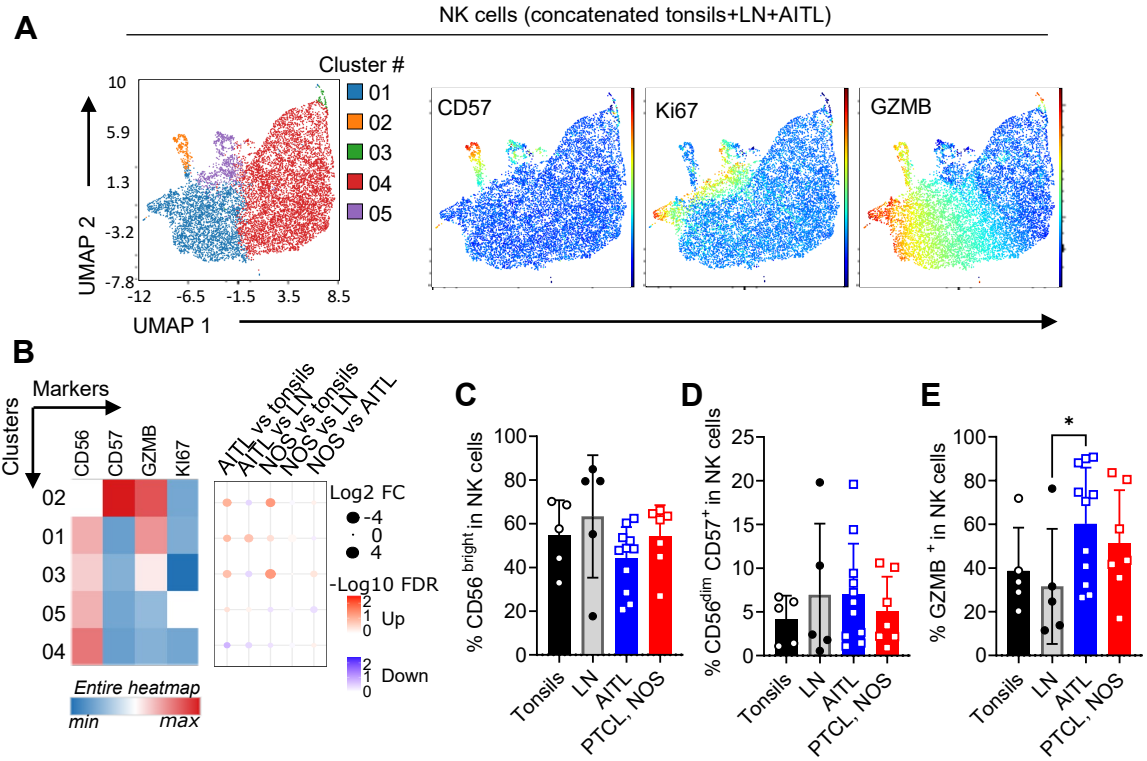
A
NK cells (concatenated tonsils+LN+AITL)
Cluster #
01
02
03
04
05
UMAP 2
UMAP 1
CD57
Ki67
GZMB
B
Markers
Clusters
CD56
CD57
GZMB
KI67
AITL vs tonsils
AITL vs LN
NOS vs tonsils
NOS vs LN
NOS vs AITL
Log2 FC
-Log10 FDR
Up
Down
Entire heatmap
min
max
C
% CD56bright in NK cells
D
% CD56dim CD57+ in NK cells
E
% GZMB + in NK cells
Tonsils
LN
AITL
PTCL, NOS

Figure S6

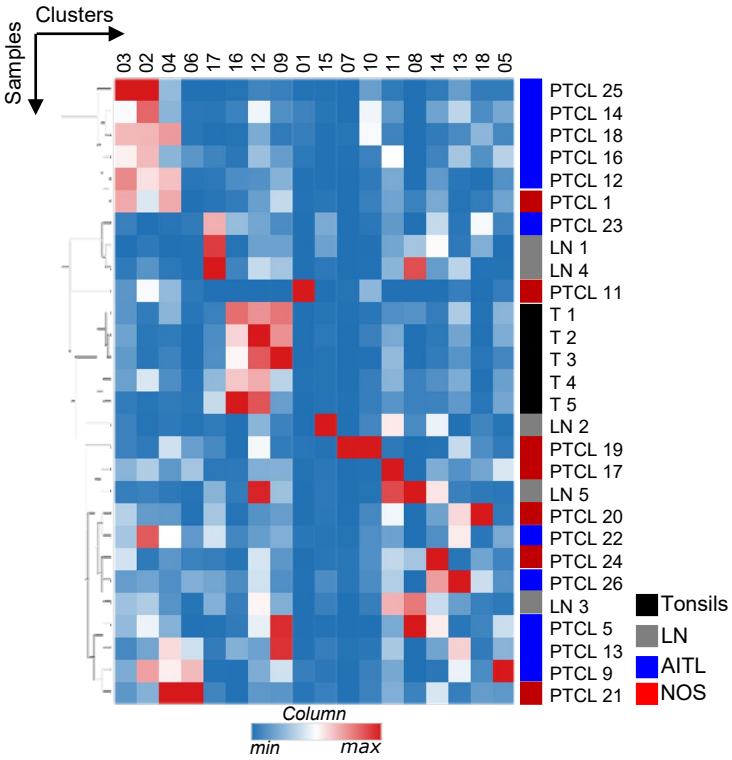
Clusters
Samples
03
02
04
06
17
16
12
09
01
15
07
10
11
08
14
13
18
05
PTCL 25
PTCL 14
PTCL 18
PTCL 16
PTCL 12
PTCL 1
PTCL 23
LN 1
LN 4
PTCL 11
T 1
T 2
T 3
T 4
T 5
LN 2
PTCL 19
PTCL 17
LN 5
PTCL 20
PTCL 22
PTCL 24
PTCL 26
LN 3
PTCL 5
PTCL 13
PTCL 9
PTCL 21
Tonsils
LN
AITL
NOS
Column
min
max

Figure S7

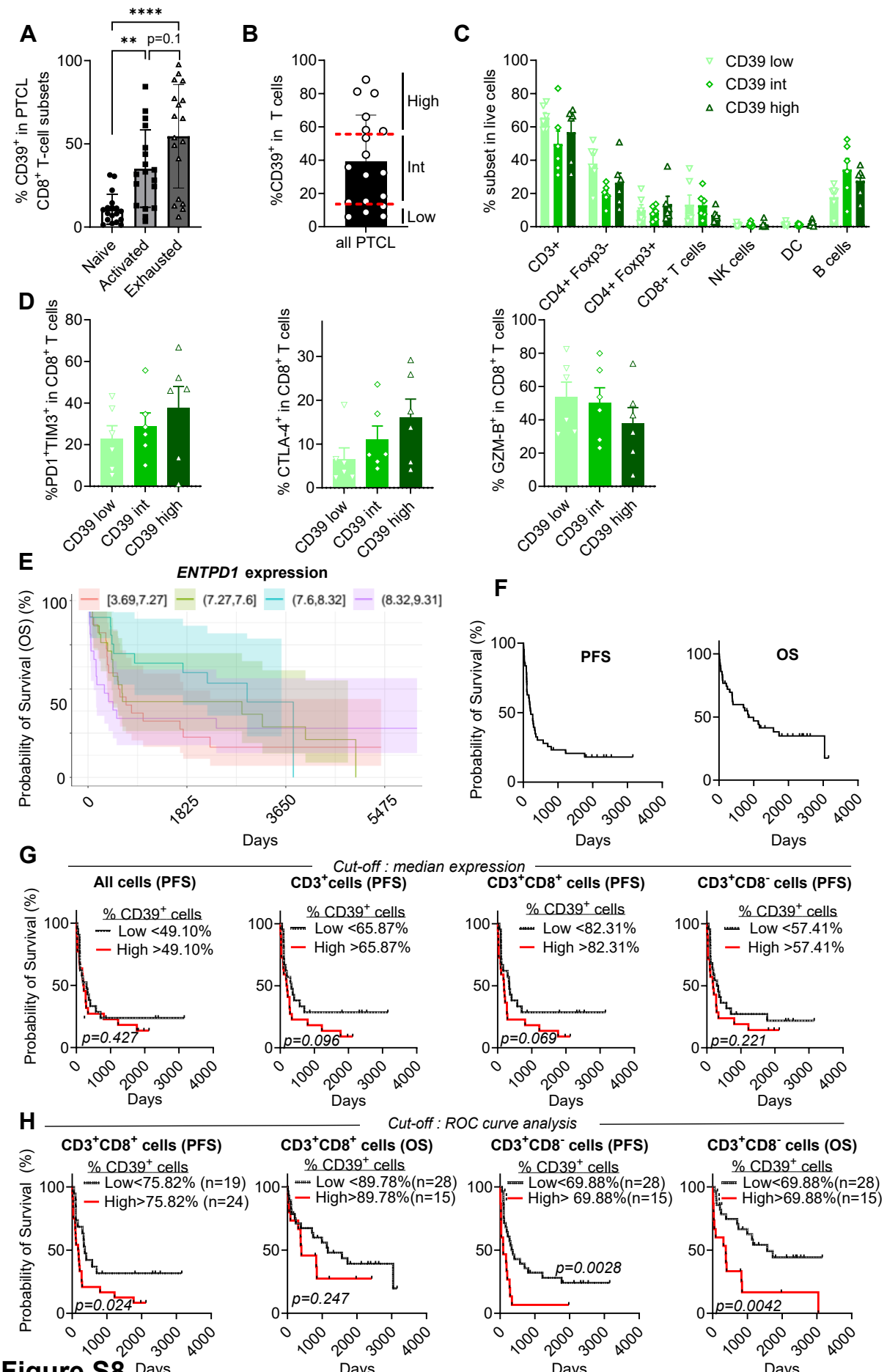
A
****
** p=0.1
% CD39+ in PTCL CD8+ T-cell subsets
Naive
Activated
Exhausted
B
%CD39+ in T cells
High
Int
Low
all PTCL
C
CD39 low
CD39 int
CD39 high
% subset in live cells
CD3+
CD4+ Foxp3-
CD4+ Foxp3+
CD8+ T cells
NK cells
DC
B cells
D
%PD1+TIM3+ in CD8+ T cells
% CTLA-4+ in CD8+ T cells
% GZM-B+ in CD8+ T cells
CD39 low
CD39 int
CD39 high
E
ENTPD1 expression
[3.69,7.27]
(7.27,7.6]
(7.6,8.32]
(8.32,9.31]
Probability of Survival (OS) (%)
Days
F
PFS
OS
Probability of Survival (%)
Days
G
Cut-off : median expression
All cells (PFS)
CD3+cells (PFS)
CD3+CD8+ cells (PFS)
CD3+CD8- cells (PFS)
% CD39+ cells
Low <49.10%
High >49.10%
p=0.427
Low <65.87%
High >65.87%
p=0.096
Low <82.31%
High >82.31%
p=0.069
Low <57.41%
High >57.41%
p=0.221
Probability of Survival (%)
Days
H
Cut-off : ROC curve analysis
CD3+CD8+ cells (PFS)
CD3+CD8+ cells (OS)
CD3+CD8- cells (PFS)
CD3+CD8- cells (OS)
% CD39+ cells
Low<75.82% (n=19)
High>75.82% (n=24)
p=0.024
Low <89.78%(n=28)
High>89.78%(n=15)
p=0.247
Low<69.88%(n=28)
High> 69.88%(n=15)
p=0.0028
Low<69.88%(n=28)
High>69.88%(n=15)
p=0.0042
Probability of Survival (%)
Days

Figure S8

Supplementary figure legends

Figure S1. Spectral FACS analyses of PTCL samples (A) Kaplan-Meier curves of PFS and OS in the 18-patient flow cytometry cohort. (B) Samples were stained for FACS and analyzed using unsupervised clustering after manual gating on total live cells. The heatmap shows unsupervised hierarchical distribution of clusters between samples (normalized by column).

Figure S2. Manual gating strategy. An example of gating strategy in an AITL sample is shown. This strategy was used for both supervised and unsupervised analyses.

Figure S3. Perturbations of Tconv cell phenotype in PTCL patients. FACS analyses following manual gating on live $CD3^+CD4^+Foxp3^-$ Tconv cells. (A) Expression of selected markers projected on UMAP. (B) Dot plots showing heterogeneous expression of checkpoint molecules in selected patients, following manual gating on live Tconv cells. (C) Heatmap showing unsupervised hierarchical separation of clusters between samples (normalized by column).

Figure S4. Analysis of surface CD3-negative live cells. Unsupervised clustering analyses following manual gating on live $CD3^-$ cells in tonsils, reactive LN and AITL samples, and concatenation using the same number of cells in each sample. (A) FlowSOM distribution of clusters and expression of selected markers projected on UMAP. (B) Heatmap showing hierarchical clustering and expression (normalized by column) of indicated markers in FlowSOM clusters. (C) Heatmap showing unsupervised hierarchical separation of clusters between samples (normalized by column). (D) Dot plots showing expression of the indicated markers in selected patients.

Figure S5. Analysis of Treg cells. (A) Proportion of $Foxp3^+$ regulatory T cells (Treg cells) among live cells (left) and among $CD4^+$ T cells (right) following manual gating. (B) UMAP visualization, FlowSOM distribution of clusters and projection of selected markers in concatenated samples. (C) Heatmap showing hierarchical clustering and expression (normalized across markers) of indicated markers in FlowSOM clusters, and their differential

enrichment between groups. (D) Proportion of CD45RA$^+$TCF1$^+$ naïve Treg cells among total Treg cells. In A, mean +/- SEM is shown; each dot represents a sample. Kruskal-Wallis tests were used. * $p < 0.05$, ** $p < 0.005$.

Figure S6. Analysis of NK cells. (A) UMAP visualization, FlowSOM distribution of clusters and projection of selected markers in concatenated samples upon gating on live CD7$^+$CD56$^+$ Natural Killer (NK) cells. (B) Heatmap showing hierarchical clustering and expression (normalized across markers) of indicated markers in FlowSOM clusters, and their differential enrichment between groups. No statistical difference in cluster representation between samples was found. (C-E) Proportions of CD56^{bright} (B), CD56^{dim} (C) and GzmB$^+$ (E) NK cells upon manual gating. Kruskal-Wallis tests were used. * $p < 0.05$.

Figure S7. CD8$^+$ T cells in PTCL. FACS analyses following manual gating on live CD8$^+$ T cells and random selection of an equal number of cells between each group. The heatmap shows unsupervised hierarchical separation of clusters between samples (normalized by column).

Figure S8. CD39 expression and prognosis value in PTCL. (A) Proportion of CD39$^+$ cells among naïve (CD45RA$^+$), activated (CD45RA$^-$PD-1$^-$TIM3$^-$) and exhausted (PD-1$^+$TIM3$^+$) CD8$^+$ T cells in the 18 PTCL samples. (B) Proportion of CD39$^+$ cells among live T cells. Dashed lines denote the 3 groups of patients according to their level of CD39 expression (low, intermediate, high). (C) Distribution of immune cell subsets in the 3 groups of patients. (D) Proportion of PD-1$^+$TIM3$^+$ exhausted CD8$^+$ T cells, CTLA-4$^+$ CD8$^+$ T cells and GzmB$^+$ CD8$^+$ T cells. (E) Kaplan-Meier curves of OS in patients from the TENOMIC AITL cohort (n=85). *ENTPD1* (CD39) mRNA expression was split in quartiles. (F) Kaplan-Meier curves of PFS and OS in the overall 43-AITL patient cohort used for multi-IF analyses. (G) Kaplan-Meier curves of PFS in different cell populations. CD39 high and low populations were split based on median expression across samples. (H) Kaplan-Meier curves of PFS and OS in CD3$^+$CD8$^+$ and CD3$^+$CD8$^-$ populations. CD39 *high* and *low* samples were split following ROC curve analyses.

	N patients with available data	n	%
Age median [range] Age <60y Age ≥60y Age ≥70y	18 67 [39-82]	 6 5 7	 33 28 39
Sex Male Female	18	 8 10	 44 56
Type of PTCL AITL PTCL-NOS	18	 11 7	 61 39
Ann Arbor stage I II III IV	17	 0 0 7 10	 0 0 41 59
ECOG performance status 0 1 2 3 4	15	 6 3 2 1 3	 40 20 13 7 20
B symptoms No Yes	16	 4 12	 25 75
Extranodal sites 0 1 ≥2	15	 6 3 6	 40 20 40
Bone marrow involvement No Yes	11	 9 2	 82 8
LDH ≤ Upper limit of normal > Upper limit of normal	14	 3 11	 21 79
Hemoglobin ≥ 12g/dL <12g/dL	13	 7 6	 54 46
IPI 0 1 2 3 4 5 IPI (simplified) <3 ≥3	15 17	 0 1 0 10 3 1 1 16	 0 7 0 67 20 7 6 94

PIT	15		
0		1	7
1		2	13
2		8	53
3		4	27
4		0	0
PIT (simplified)	16		
<2		3	19
≥2		13	81
PIAI (simplified)			
<2	16	0	0
≥2		16	100

Supplementary Table 1. Clinical characteristics of the PTCL cohort used in spectral flow cytometry analyses

Sample ID	Sex	Age (years)	Diagnosis	Clinical phenotying data	Institutional source	Year of collection	Storage time (month)	Tissue Origin
PTCL 1	F	67	NOS	Missing Data	Lyon-Sud hospital	1996	300	LN
PTCL 5	M	67	AITL	CD2+ CD3+ CD7+ CD4+ CD8- CD10- BCL6low PDL1low CXCL13-	Lyon-Sud hospital	2019	19	LN
PTCL 9	F	62	AITL	CD2+ CD3+CD5+ CD4+ CD8- CD7+ PD-1+ ICOS+ CXCL13+ CD10- BCL6- CD30+(15%)	Lyon-Sud hospital	2019	28	LN
PTCL 11	M	55	NOS	CD2+ CD3+ CD5- CD7- CD4- CD8- CD30low ICOS +/- PD-1 +/- EMA- CD10- ALK1- GZMB+ Perforin+ TiA1+	CEVI group	2014	91	LN
PTCL 12	M	49	AITL	CD2+ CD3+ CD5+ CD7+/- CD4+ CD8- TCRb1+ CD10- BCL6- PD1+ ICOS+ CXCL13- CD30- CD25- CD103+ CD56- Perforine- TiA1-	CEVI group	2015	76	LN
PTCL 13	M	64	AITL	CD20+ CD79a- PAX5- CD3+ CD2+ CD5+ CD7- CD4+ CD8- TCRb1+ CD10- ICOS+ PD1+ BCL6+(heterogeneous) CXCL13+ CD30(10%) CD25-	CEVI group	2017	53	LN
PTCL 14	M	57	AITL	CD3+ CD4+/- CD8- CD5+ CD2+ CD7+ PD1+ CXCL13+(partial) ICOS+(heterogeneous) CD15-	CEVI group	2019	30	LN
PTCL 16	F	75	AITL	CD3+ CD4+ CD5+ PD1+ CD7low CD10- CXCL13-	CEVI group	2015	79	LN
PTCL 17	F	69	NOS	CD3+ CD4+ CD8- CD5+ CD7- CD30- CD10- PD-1 +/- CXCL13-	CEVI group	2016	56	LN
PTCL 18	F	71	AITL	CD3+ CD4+ CD8- CD7low PD1+ CXCL13+ CD10+(heterogeneous) BCL6-	CEVI group	2018	37	LN
PTCL 19	M	80	NOS	CD3+ CD4+ CD7+ Ki67+	CEVI group	2019	44	LN
PTCL 20	M	74	NOS	CD3+ CD4+ CD7+ CD10-	CEVI group	2017	56	LN
PTCL 21	F	82	NOS	CD3+ CD5low CD4+ CD8- PD1+(heterogeneous) CXLC13+(heterogeneous) CD30-	CEVI group	2021	9	LN
PTCL 22	F	46	AITL	CD3+ CD4+ CD10+ PD1+ CD7low	CEVI group	2019	44	LN
PTCL 23	M	39	AITL	CD3+ CD4+ CD10+ PD1+ CD7-	CEVI group	2015	78	LN
PTCL 24	F	58	NOS	CD3+ CD4+ CD7- PD1- CD10-	CEVI group	2019	25	LN
PTCL 25	F	75	AITL	CD3+ CD4+ CD7- PD1+ CD10+ Bcl6+	CEVI group	2016	62	LN
PTCL 26	F	73	AITL	CD3+ CD4+ CD7+ PD1+ CD10- Bcl6-	CEVI group	2017	53	LN
LN 1	F	50	Reactive LN	Follicular hyperplasia, no T/B clonality	Lyon-Sud hospital	2019	49	LN
LN 2	M	77	Reactive LN	No abnormalities, no inflammation.	Lyon-Sud hospital	2020	42	LN
LN 3	M	57	Reactive LN	Follicular hyperplasia in a patient cured (complete response) from Hodgkin lymphoma.	Lyon-Sud hospital	2017	78	LN

LN 4	F	51	Reactive LN	Follicular hyperplasia, no T/B clonality. Suggestive of lupus lymphadenopathy	Lyon-Sud hospital	2019	56	LN
LN 5	F	71	Reactive LN	Lymphadenopathy, benign, no tumor cells, no B clonality	Lyon-Sud hospital	2023	9	LN
Tonsil 1	F	8	Tonsil	NA	Clinique du parc, Lyon	2020	16	Tonsil
Tonsil 2	M	7	Tonsil	NA	Clinique du parc, Lyon	2020	16	Tonsil
Tonsil 3	M	7	Tonsil	NA	Clinique du parc, Lyon	2020	8	Tonsil
Tonsil 4	M	6	Tonsil	NA	Clinique du parc, Lyon	2021	2	Tonsil
Tonsil 5	F	5	Tonsil	NA	Clinique du parc, Lyon	2021	1	Tonsil

Supplementary Table 2. Individual clinical immunophenotyping data of the spectral flow cytometry cohort

	N patients with available data	n	%
Age median [range] Age <60y Age ≥60y Age ≥70y	43	 69 [30-87] 11 11 21	 26 26 49
Sex Male Female	43	 24 19	 56 44
Type of PTCL AITL PTCL-NOS	43	 43 0	 100 0
Ann Arbor stage I II III IV	42	 0 2 19 21	 0 5 45 50
ECOG performance status 0 1 2 3 4	41	 4 13 17 4 3	 10 32 41 29 7
B symptoms No Yes	43	 9 34	 21 79
Extranodal sites 0 1 ≥2	42	 20 12 10	 48 28 24
Bone marrow involvement No Yes	33	 16 17	 49 51
LDH ≤ Upper limit of normal > Upper limit of normal	41	 5 36	 12 88
Hemoglobin ≥ 12g/dL <12g/dL	40	 17 23	 42 58
Platelets ≥ 150 000/mm^3 <150 000/mm^3	39	 34 5	 87 13
Monocytes ≥800/mm^3 <800/mm^3	34	 14 20	 41 59

IPI	41		
0		0	0
1		1	2
2		6	15
3		13	32
4		18	44
5		3	7
IPI (simplified)	41		
<3		7	17
≥3		34	83
PIT	32		
0		0	0
1		4	13
2		10	33
3		13	38
4		5	15
PIT (simplified)	41		
<2		4	10
≥2		37	90
PIAI	39		
0		2	7
1		6	16
2		10	27
3		14	33
4		7	18
5		0	0
PIAI (simplified)	43		
<2		8	19
≥2		35	81

Supplementary Table 3. Clinical characteristics of the PTCL cohort used in multi-IF analyses

AITL Patient ID	Sex	Age	Diagnosis	Year of collection	Source of the sample	Tissue origin
AITL 1	M	82	AITL	2012 to 2021	Lyon	Lymph node
AITL 2	M	58	AITL			
AITL 3	F	68	AITL			
AITL 4	M	53	AITL			
AITL 5	F	30	AITL			
AITL 6	M	70	AITL			
AITL 7	M	86	AITL			
AITL 8	F	77	AITL			
AITL 9	F	48	AITL			
AITL 10	M	86	AITL			
AITL 11	M	73	AITL			
AITL 12	M	86	AITL			
AITL 13	M	75	AITL			
AITL 14	F	76	AITL			
AITL 15	F	81	AITL			
AITL 16	M	76	AITL			
AITL 17	F	70	AITL			
AITL 18	M	53	AITL			
AITL 19	F	75	AITL			
AITL 20	F	67	AITL			
AITL 21	M	62	AITL			
AITL 22	M	80	AITL			
AITL 23	F	78	AITL			
AITL 24	M	67	AITL			
AITL 25	M	69	AITL/TFH			
AITL 26	M	48	AITL			
AITL 27	F	62	AITL/TFH			
AITL 28	M	68	AITL			
AITL 29	M	75	AITL			
AITL 30	M	64	AITL			
AITL 31	F	57	AITL			
AITL 32	M	54	AITL			
AITL 33	F	49	AITL			
AITL 34	M	71	AITL			
AITL 35	F	80	AITL			
AITL 36	F	75	AITL			
AITL 37	F	50	AITL			
AITL 38	M	61	AITL			
AITL 39	M	53	AITL			
AITL 40	F	87	AITL/TFH			
AITL 41	F	84	AITL			
AITL 42	F	68	AITL			
AITL 43	M	66	AITL/TFH			

Supplementary Table 4. Individual sample data from the PTCL cohort used in multi-IF analyses

Reagent	Source	Identifier	Working concentration
Live/Dead Blue	Thermo Fisher Scientific	L23105	1/1000
BV711 Rat Anti-Human CXCR5 (CD185) (RF8B2)	BD Biosciences	740737	1/80
cFluor® YG584 Anti-Human CD4 (SK3)	Cytek	SKU R7-20041	1/100
Spark NIR™ 685 anti-human CD20 Antibody (2H7)	BioLegend	302366	1/40
APC/Fire™ 750 anti-human CD39 Antibody (A1)	BioLegend	328230	1/80
Pacific Blue™ anti-human CD57 Antibody (HNK-1)	BioLegend	359608	1/80
APC/Fire™ 810 anti-human CD3 Antibody (SK7)	BioLegend	344858	1/80
Vio® Bright FITC anti-human CD120b (TNF-RII) Antibody,REAfinity™ (REA520)	Miltenyi Biotec	130-119-777	1/50
PE/Dazzle™ 594 anti-human TIGIT (VSTM3) Antibody (A15153G)	BioLegend	372716	1/40
PE/Cy5.5 LAG-3 Antibody (17B4)	Novus Biologicals	NBP1-97657PECY55	1/3200
PerCP-Vio® 700 anti-human CD163 Antibody, REAfinity™ (REA812)	Miltenyi Biotec	130-112-133	1/100
PerCP-Cy™5.5 Mouse Anti-Human TCR γδ (B1)	BD Biosciences	564157	1/20
CD137 Antibody, anti-human, APC, REAfinity™ (REA765)	Miltenyi Biotec	130-110-764	1/50
BUV563 Mouse Anti-Human CD7 (M-T701)	BD Biosciences	741355	1/80
Brilliant Violet 570™ anti-human CD45RA Antibody (HI100)	BioLegend	304132	1/40
BV605 Mouse Anti-Human CD56 (NCAM16.2)	BD Biosciences	562780	1/40
BUV805 Mouse Anti-Human CD8 (SK1)	BD Biosciences	612889	1/80
BB515 Mouse Anti-Human CD11c (B-ly6)	BD Biosciences	564490	1/40
BV510 Mouse Anti-Human NKG2A (CD159a) (131411)	BD Biosciences	747922	1/20
BUV661 Mouse Anti-Human CD226 (DX11)	BD Biosciences	749934	1/40
BUV737 Mouse Anti-Human CD134 (ACT35)	BD Biosciences	749286	1/40
BV750 Mouse Anti-Human CD278 (ICOS) (DX29)	BD Biosciences	746858	1/40
BUV615 Mouse Anti-Human TIM-3 (CD366) (7D3)	BD Biosciences	752363	1/20
BV786 Mouse Anti-Human CD279 (PD-1) (EH12.1)	BD Biosciences	563789	1/40
BUV496 Mouse Anti-Human CD10 (MEM-78)	BD Biosciences	750190	1/40
Alexa Fluor® 647 Mouse Anti-TCF-7/TCF-1 (S33-966)	BD Biosciences	566693	1/20
PE-Cyanine5 anti-human FOXP3 Monoclonal Antibody (PCH101)	Thermo Fisher Scientific	15-4776-42	1/40
Alexa Fluor® 700 Mouse anti-Human Granzyme B (GB11)	BD Biosciences	560213	1/80
PE-Cyanine7 anti-human CD152 (CTLA-4) (14D3)	Thermo Fisher Scientific	25-1529-42	1/40
PE Mouse Anti-EOMES (X4-83)	BD Biosciences	566749	1/20
BV650 Mouse Anti-T-bet (O4-46)	BD Biosciences	564142	1/40
BUV395 Mouse Anti-Ki-67 (B56)	BD Biosciences	564071	1/40
BV421 Mouse Anti-Bcl-6 (K112-91)	BD Biosciences	563363	1/40

Reagent	Source	Identifier	Working concentration
Mouse anti-human CD3 (polyclonal)	Agilent	A052	1/100
Mouse anti-human CD8 (C8/144B)	Agilent	M7103	1/40
Rabbit anti-human CD39 (polyclonal)	Sigma Aldrich	HPA014067	1/50

Supplementary Table 5. FACS and multi-IF Abs used in this study

Sample ID	Diagnosis	Number of cells in the sample	Number of labeled cells	Number of acquired events	% of live cells	Number of live cells processed
PTCL 1	NOS	25,000,000	1,000,000	237,714	67.0%	159,353
PTCL 5	AITL	3,000,000	1,000,000	141,138	35.9%	50,690
PTCL 9	AITL	4,000,000	1,000,000	263,894	82.1%	216,700
PTCL 11	NOS	2,000,000	1,000,000	43,133	48.5%	20,935
PTCL 12	AITL	2,000,000	1,000,000	281,939	44.6%	125,630
PTCL 13	AITL	10,000,000	1,000,000	247,175	81.2%	200,599
PTCL 14	AITL	9,000,000	1,000,000	81,989	85.7%	70,293
PTCL 16	AITL	3,000,000	1,000,000	273,702	67.0%	183,471
PTCL 17	NOS	7 500,000	1,000,000	228,216	88.1%	201,156
PTCL 18	AITL	5,000,000	1,000,000	360,963	43.2%	155,963
PTCL 19	NOS	3,000,000	1,000,000	406,876	68.9%	280,518
PTCL 20	NOS	4,000,000	1,000,000	524,588	76.8%	402,729
PTCL 21	NOS	4,000,000	1,000,000	344,937	64.4%	222,123
PTCL 22	AITL	6,000,000	1,000,000	153,189	65.5%	100,366
PTCL 23	AITL	8,000,000	1,000,000	370,228	79.9%	295,805
PTCL 24	NOS	1,000,000	1,000,000	154,338	63.5%	98,070
PTCL 25	AITL	7,000,000	1,000,000	394,985	66.1%	261,057
PTCL 26	AITL	3,000,000	1,000,000	305,753	65.7%	200,795
LN 1	Reactive LN	8,230,000	1,000,000	106,181	89.4%	94,952
LN 2	Reactive LN	6,070,000	1,000,000	188,014	78.1%	146,884
LN 3	Reactive LN	9,100,000	1,000,000	194,612	87.5%	170,287
LN 4	Reactive LN	467,000	467,000	32,533	90.6%	29,489
LN 5	Reactive LN	8,230,000	1,000,000	155,779	91.9%	143,159
Tonsil 1	Tonsil	26,000,000	1,000,000	156,041	92.3%	144,077
Tonsil 2	Tonsil	13,000,000	1,000,000	149,960	90.9%	136,332
Tonsil 3	Tonsil	43,000,000	1,000,000	223,181	89.5%	199,819
Tonsil 4	Tonsil	44,000,000	1,000,000	140,042	86.0%	120,410
Tonsil 5	Tonsil	120,000,000	1,000,000	226,043	86.8%	196,244

Supplementary Table 6. Individual cell counts before and after staining for spectral flow cytometry analyses

Sample ID	Live cells		T conv cells		CD8+ T cells	
	Total count	Included in unsupervised analysis	Total count	Included in unsupervised analysis	Total count	Included in unsupervised analysis
PTCL 1	159,353	83,538	26,664	16,740	55,500	4,424
PTCL 5	50,690	50,690	16,857	10,653	2,667	2,667
PTCL 9	216,700	53,161	33,258	10,653	17,059	2,815
PTCL 11	20,935	20,935	6,553	6,553	2,892	2,892
PTCL 12	125,630	53,161	56,625	10,653	7,798	2,815
PTCL 13	200,599	53,161	19,182	10,653	7,331	2,815
PTCL 14	70,293	53,161	16,431	10,653	5,349	2,815
PTCL 16	183,471	53,161	37,869	10,653	28,570	2,815
PTCL 17	201,156	83,538	54,418	16,740	33,907	4,424
PTCL 18	155,963	53,161	27,635	10,653	40,488	2,815
PTCL 19	280,518	83,538	30,368	16,740	18,433	4,424
PTCL 20	402,729	83,538	180,200	16,740	13,469	4,424
PTCL 21	222,123	83,538	47,824	16,740	11,964	4,424
PTCL 22	100,366	53,161	18,438	10,653	8,170	2,815
PTCL 23	295,805	53,161	150,710	10,653	17,058	2,815
PTCL 24	98,070	83,538	50,996	16,740	2,994	2,994
PTCL 25	261,057	53,161	93,769	10,653	71,063	2,815
PTCL 26	200,795	53,161	57,203	10,653	6,126	2,815
LN 1	94,952	94,952	49,643	23,436	13,761	6,194
LN 2	146,884	116,954	50,197	23,436	21,358	6,194
LN 3	170,287	116,954	26,505	23,436	5,556	5,556
LN 4	29,489	29,489	9,941	9,941	2,986	2,986
LN 5	143,159	116,954	33,121	23,436	8,086	6,194
Tonsil 1	144,077	116,954	27,352	23,436	5,191	5,191
Tonsil 2	136,332	116,954	19,087	19,087	6,934	6,194
Tonsil 3	199,819	116,954	37,128	23,436	10,299	6,194
Tonsil 4	120,410	116,954	10,478	10,478	4,288	4,288
Tonsil 5	196,244	116,954	23,139	23,139	4,258	4,258

Supplementary Table 7. Number of cells of each indicated subset used for unsupervised analyses following down-sampling and concatenation

Sample ID	Treg cells		NK cells	
	Total count	Included in unsupervised analysis	Total count	Included in unsupervised analysis
PTCL 1	8,277	1,243	1,196	447
PTCL 5	8,156	791	1,385	284
PTCL 9	11,144	791	695	284
PTCL 11	1,767	1,243	323	323
PTCL 12	12,029	791	224	224
PTCL 13	27,226	791	264	264
PTCL 14	3,109	791	491	284
PTCL 16	13,840	791	3,339	284
PTCL 17	18,761	1,243	4,068	447
PTCL 18	19,005	791	5,618	284
PTCL 19	39,055	1,243	1,197	447
PTCL 20	91,788	1,243	691	447
PTCL 21	24,211	1,243	12,503	447
PTCL 22	2,957	791	990	284
PTCL 23	20,316	791	680	284
PTCL 24	2,108	1,243	296	296
PTCL 25	10,480	791	3,381	284
PTCL 26	72,999	791	1,003	284
LN 1	3,778	1,741	503	503
LN 2	4,344	1,741	232	232
LN 3	1,359	1,359	1,129	626
LN 4	634	634	29	29
LN 5	4,499	1741	1,326	626
Tonsil 1	1,840	1,741	276	276
Tonsil 2	1,377	1,377	702	626
Tonsil 3	2,746	1,741	488	488
Tonsil 4	709	709	645	626
Tonsil 5	2,034	1,741	1,019	626

Supplementary Table 7 (continued). Number of cells of each indicated subset used for unsupervised analyses following down-sampling and concatenation

Sample ID	Diagnosis	Putative malignant aberrant phenotype 1	Putative malignant aberrant phenotype 2
PTCL 1	NOS	**Not identified**	Not identified
PTCL 5	AITL	CD3+CD4+CD8-CD7-CD10+/-PD1+TIM3+ICOS+/-LAG3+/-	Not identified
PTCL 9	AITL	**Not identified** (all T cells are PD1+ICOS+CTLA4+TIGIT+)	Not identified
PTCL 11	NOS	CD3+CD4-CD8-CD7-CD10+PD1+TIM3+ICOS-GZMB+	Not identified
PTCL 12	AITL	CD3+CD4+CD8-CD7-PD1+ICOS+CTLA4+EOMES-	CD3+CD4+CD8-CD7-PD1+ICOS+CTLA4-EOMES+
PTCL 13	AITL	CD3+CD4+CD8-CD7-PD1+ICOS+CTLA4+	CD3+CD4-CD8-CD7- PD1+ICOS+CTLA4bright
PTCL 14	AITL	CD3+CD4+CD8-CD7+CD10-PD1+ICOS+CTLA4+OX40+Ki67+	CD3+CD4+CD8-CD10+PD1+ICOS+CTLA4-OX40-Ki67- **AND** Ki67+ cells, not other specified
PTCL 16	AITL	CD3+CD4+CD8-CD7-CD10+PD1+ICOS+CTLA4+OX40+	Not identified
PTCL 17	NOS	CD3+CD4+CD8-CD7-CD10+PD1+ICOS+/-CTLA4+/-EOMES+/-	CD3+CD4-CD8-CD7-CD10-PD1+ICOS+/-CTLA4+/-EOMES+/-
PTCL 18	AITL	CD3+CD4+CD7+PD1+ICOS+CTLA4+OX40+	Not identified
PTCL 19	NOS	CD3+CD4+CD8-CD7+PD1+ICOS+Ki67+	CD3+CD4-CD8-CD7-PD1+ICOS+Ki67-
PTCL 20	NOS	CD3+CD4+CD8-CD7-TCRgd+PD1+/-ICOS+/-	Not identified
PTCL 21	NOS	CD3+CD4+CD8-CD7-PD1+ICOS+/-EOMES+/-	CD3-CD4+CD8-CD7- PD1-GZMB+EOMES+FOXP3+
PTCL 22	AITL	CD3+CD4+CD8-CD7-CD10-PD1+ICOS+CTLA4+	CD3-CD4+CD8-CD7-CD10+PD1+ICOS+CTLA4+
PTCL 23	AITL	CD3+CD4+CD8-CD7-CD10+PD1+ICOS+	Not identified
PTCL 24	NOS	CD3+CD4+CD8-CD7-PD1-ICOS+LAG3-	CD3+CD4+CD8-CD7-PD1-ICOS+LAG3+
PTCL 25	AITL	CD3+CD4+CD8-CD7-CD10+PD1+ICOS+CTLA4+OX40+	CD3-CD4-CD8-FOXP3+CD39+
PTCL 26	AITL	CD3+CD4+CD8-CD7-CD10+PD1+ICOS+CTLA4+OX40+EOMES+	CD3+CD4+CD8-CD7+CD10+PD1+ICOS+CTLA4+OX40+EOMES-

Supplementary Table 8. Putative identification of neoplastic phenotypes in PTCL samples.

Supplemental methods

Flow cytometry staining

After thawing in a water bath at 37°C, the cell suspensions were washed in RPMI 1640 W/HEPES W/GLUTAMAX-I (supplemented with 10% FBS; Penicillin/Streptomycin; Non-Essential Amino Acids; Sodium Pyruvate and β-Mercaptoethanol, all from Thermo Fisher). 1 million cells per sample were stained with viability dye for 15 min at room temperature (RT), then incubated with Human FC block for 10 min at RT. Cells were then incubated with CXCR5 antibody mix in FACS buffer (PBS1X with 2.5 mM EDTA and 3% FBS) for 20 min at 37°C, then with surface marker antibodies mixed in FACS buffer and brillant stain buffer (BD) for 30 min at RT in the dark. Cells were then fixed and permeabilized using the eBioscience Foxp3/Transcription Factor Staining Buffer Set (Thermo Fisher Scientific) according to manufacturer's instructions. Cells were finally incubated with intracellular marker antibodies mix for 20 min at 4°C.

Flow cytometry unsupervised analyses

Briefly, each cell subset was gated manually (Live cells, sCD3-negative cells, Tconv cells, Treg cells, CD8+ T cells and NK cells). Prior to concatenation, we used down-sampling to avoid over-representation of one group over the others, which could lead to the identification of poorly representative clusters. The total number of cells in each tissue (tonsils, reactive LN, AITL and PTCL, NOS) was therefore made identical by reducing the number of events to that of the smaller sample. Details on the number of events processed in each case can be found in Tables S3 and S4. Following concatenation, 2-dimensional reduction through Uniform Manifold Approximation and Projection (UMAP) and hierarchical clustering through FlowSOM were used.

Tissue micro-arrays and multi-IF protocol

TMA blocks were generated by punching 1 mm cores from FFPE tissue samples using a Tissue Arrayer MiniCore instrument with TMADesigner® 2 Software from ALPHELYS. Three

1 mm cores were taken from each patient sample. The three-plex mIF assay was first optimized as previously described [23]. The standard seven-color TSA protocol template on the BOND RXm was used with modifications. TMAs underwent an initial antigen retrieval step of ER1 at 100°C for 20 min, a dispensing of the TSA reagents (incubation time of 30 min), and DAPI staining at a volume of 150 µL for 5 min. The following sequence was used: anti-CD3+OPAL 570 (position 3), anti-CD8+OPAL 520 (position 4), anti-CD39+OPAL 690 (position 5). All antibodies were diluted using Akoya's antibody diluent/blocking buffer. Slides were imaged using the Vectra Polaris spectral imaging system (Perkin Elmer) at 20X or 40X for TMA. Scans were visualized with the Phenochart software where autofluorescence can be directly removed.

Multi-IF data processing

TMA cores were excluded if one of the following criteria was present: large part or whole of core lost; poor quality staining; or widespread necrosis. Cell phenotypes could be analyzed in the 43 patients. In 6 of them, it was evaluated in one TMA core. For the others, the results retained for each patient were the median of the 2 or 3 TMA cores. Images were spectrally separated with a synthetic algorithm in InForm version 2.4.8 (Akoya Biosciences). Cell phenotypes were identified and counted using image analysis in InForm. Six TMA cores representing the heterogeneous nature of AITL, were selected to train machine learning algorithms for tissue segmentation, cell segmentation and cell phenotyping. First, the tissue was divided into tumor or non-tumor compartments using the tissue segmentation setting by drawing different areas as different categories. Then, cell segmentation was performed using DAPI counterstaining, using the adaptive cell segmentation setting in InForm software. The splitting parameter was adjusted to segment crowded and overlapping cells. Membrane staining was selected to assist in nuclear segmentation. Seven cell phenotypes were analyzed: total T lymphocytes ($CD3^+$), $CD8^+$ T lymphocytes ($CD3^+CD8^+$), non-$CD8^+$ T lymphocytes ($CD3^+CD8^-$), total cells expressing CD39 ($CD39^+$), total T lymphocytes expressing CD39

($CD3^+CD39^+$), $CD8^+$ T lymphocytes expressing CD39 ($CD3^+CD8^+CD39^+$) and non-$CD8^+$ T lymphocytes expressing CD39 ($CD3^+CD8^-CD39^+$). When the training was completed, it was applied to a set of cases to verify that it was working properly. These parameters were then applied to all TMA cores and the percentage of cells according to their phenotypes was calculated using the R version 4.2.1 software.